Online measurement techniques for nanocellulose films and coatings

Aayush Kumar Jaiswal

Master thesis

Laboratory of Paper Coating and Converting

Faculty of Science and Engineering

Åbo Akademi University

March 2019

Aayush Kumar Jaiswal

Supervisors:

Prof. Martti Toivakka

Laboratory of Paper Coating and Converting

Åbo Akademi University

Turku, Finland

Dr. Vinay Kumar

VTT Technical Research Centre of Finland

Espoo, Finland

Abstract

There has been an inclination in industrial coatings towards the utilization of more eco-friendly, renewable, and biodegradable solutions. Among these solutions, a material of special interest is nanocellulose, which, owing to its biodegradable and renewable nature in addition to properties such as mechanical robustness, flexibility, low density, non-toxicity, and surface modification ability, has become an extremely popular research topic.

This work dealt with non-contact measurement of coating thickness for nanocellulose-based films and coatings. Knife coating was used throughout the work. Three non-contact methods, viz. NIR spectroscopy, IR thermography, and optical confocal displacement sensing were used to measure thickness of nanocellulose coatings, both in dry and wet state. Two different types of nanocellulosic materials, namely, microfibrillated cellulose (MFC) and cellulose nanofibrils (CNF) were used in the study. Polypropylene, polyether sulfone membrane, and stainless steel were used as substrates.

Optical confocal displacement sensing was found to be the most accurate technique for measuring the thickness of MFC films with an RMS error of 9.3% for wet films and 29.1% for dry films. For CNF films, IR thermography produced best results with an RMS errors of 26.1% and 13.2% for wet and dry films respectively. As evident, the measurements were lacking industry-standard accuracy, which leaves the scope for improvement in future work.

Keywords: Online measurements, non-contact examination, nanocellulose, thin-films, coatings, thermography, NIR

Table of Contents

Preface

This work was carried out within a collaboration between VTT Technical Research Centre of Finland and Laboratory of Paper Coating and Converting (PaF), Åbo Akademi University from September 2018 to February 2019. This project has received funding from the European Union's Horizon 2020 research and innovation programme under grant agreement No 760601. The project is titled 'Nanotextured surfaces for membranes, protective textiles, friction pads and abrasive materials (NanoTextSurf)'

My heartfelt gratitude goes to both of my supervisors Prof. Martti Toivakka and Dr. Vinay Kumar for guiding me throughout the work, remotely and directly. Prof. Toivakka has been my guide since I stepped into research and he is a major influencer behind my decision to make a career in this field. Dr. Kumar has been a fantastic teacher, mentor, and most importantly an inspirational figure for me. He gave me the freedom to carry out the work on my pace and he trusted me to plan and execute all tasks independently. This experience has made me learn many skills that will help me professionally for years to come.

I would like to thank Dr. Ulla Forsström for providing me with the wonderful opportunity to carry out this work at VTT. Her support and encouragement was remarkable. I am also immensely grateful to Vesa Kunnari for his help in both technical and administrative work. I thank Dr. Heli Kangas for being a patient listener to all ideas I have.

Timo Kaljunen, Vuokko Liukkonen, and Eija Kenttä have helped me find my way through the labs. Anastasia, Alexey, and Ilona have been great friends. I thank the entire BA3503 team for making me feel welcome in the new workplace.

I would also like to acknowledge my friends Rajesh, Sonu, Debanga, Kofi, and Mukunda for their wonderful company and especially Yiran for being there all the time.

Finally, I am sincerely thankful to my family- Maa, Papa, and Bhaiya for everything they have done for me and for letting me pursue my dreams in a distant place they had not even heard of a couple of years ago.

Espoo, March 2019

Aayush Kumar Jaiswal

List of abbreviations

ALD	Atomic layer deposition
ATR	Attenuated total reflection
BC	Bacterial cellulose
BNC	Bacterial nanocellulose
BOPP	Biaxially oriented polypropylene
CFRP	Carbon fiber reinforced polymer
CMC	Carboxymethyl cellulose
CNC	Cellulose nanocrystal
CNF	Cellulose nanofiber, cellulose nanofibril
CNW	Cellulose nanowhisker
CVD	Chemical vapour deposition
DFT	Dry film thickness
DP	Degree of polymerization
DS	Degree of substitution
EMF	Electromotive force
FTIR	Fourier-transform infrared
gsm	Grams per square meter
IR	Infrared
IRT	Infrared thermography
ISO	International organization for standardization
KIT	Grease barrier test method
LCD	Liquid crystal display
LVE	Linear viscoelastic region
L&W	Lorentzen & Wettre
MCR	Modular compact rheometer
MFC	Microfibrillated cellulose, microfibrillar cellulose
NCC	Nanocrystalline cellulose
NDT	Non-destructive testing
NIR	Near infrared

NFC	Nanofibrillated cellulose, nanofibrillar cellulose
ORA	Optical reflection amplifier
PAF	Pappersförädling
PES	Polyether sulfone
PLA	Polylactic acid
PP	Polypropylene
pph	parts per hundred
PVA	Polyvinyl alcohol
RADAR	Radio detection and ranging
RMS	Root mean square
RH	Relative humidity
SNR	Signal-to-noise ratio
TAPPI	Technical Association of the Pulp & Paper Industry
TEMPO	2, 2, 6, 6,-tetramethylpiperidine-1-oxyl
WFT	Wet film thickness
WVTR	Water vapour transmission rate

1. Introduction

Quality control is an indispensable need for any large-scale manufacturing facility. For industrial coatings, ensuring good quality of coating is important from both economic and sustainability perspectives. Here, coating quality is a qualitative parameter which is a resultant function of multiple factors, such as uniformity in thickness, absence of defects, optimal coat weight application, drying strategy etc. Among these factors, the present work deals with monitoring of coating thickness measurement, which in turn, can be related to the coat weight. Modern coating processes possess the ability to precisely control the final coating thickness, and the control is not limited to the metering element alone as they also include measurement systems equipped with feedback to the metering system.

The coating industry has been utilizing various methods for online monitoring of coating thickness and/or coat weights for a long time. The choice of the measurement technique is based on the coating being applied. The used techniques can be broadly classified into two categories, viz. contact and non-contact testing. Typically, wet or uncured coating monitoring utilizes non-contact techniques and the dry or cured side may utilize either contact or non-contact devices. For reel-based coating processes, non-contact measurements are preferred but for semi-batch processes like powder coatings on automobile parts, contact testing might be chosen. In the papermaking and converting industry, the usual method of thickness and basis weight control is non-contact testing where the subject of the measurement can be either paper or coating.

In recent times, due to environmental concerns related to solvent-based coatings, there has been an inclination in the coatings industry towards the utilization of more eco-friendly, renewable, and biodegradable materials. This trend has resulted in research efforts to replace the harmful solvents with water or other environmentally benign solvents, to use bio-based coating materials, and to integrate coated products in the circular economy. As a result of efforts in the previous two decades, researchers have identified many solutions which include water-based dispersion coatings, drop-in biopolymer coatings, biocomposite and bionanocomposite coatings, etc. Among these solutions, a material of special interest is nanocellulose, which, owing to its biodegradable and renewable nature in addition to properties such as mechanical robustness, flexibility, low density, non-toxicity, and surface modification ability, has become an extremely popular research topic.

Applications for nanocellulose thin-film structures, such as stand-alone films and coatings have been explored widely in the last ten years. The manufacturing of nanocellulosic materials has matured at a rapid pace and constant research efforts are being made to enable their high-throughput processing into thin-film structures. Simultaneously, due to growing concerns related to plastic pollution, the market is gearing up for accepting nanocellulose-based products in daily life. As a result, the introduction of nanocellulose-based films and coatings in industrial processes is imminent and the need for quality control systems for such processes is also expected to arise.

No measurement methods have yet been studied specifically aimed at measuring thickness and/or coat weights for nanocellulose films and coatings. Thus, the motivation behind this work was to study online measurement techniques which could be utilized in industrial process control of nanocellulose-based films and coatings, in the near future. In order to fill this information void, the current work deals with online measurement of coating thickness for nanocellulose-based films and coatings. For this purpose, state-of-the-art industrial techniques were studied and the most suitable different techniques were selected to be tested. The three techniques were then studied experimentally using two different types of nanocellulose materials coated over three different types of substrates. The experimental matrix can be found in the table below.

Table 1: Experimental matrix for the current work

Substrates	**Film materials**
Plastic Polymer membrane Metal	Microfibrillated cellulose Nanofibrillated cellulose

2. Literature review

Coatings are applied in order to impart decorative, protective, and functional properties to products. A single coating layer may deliver multiple features, or several different coating layers may be required to achieve the desired properties. The choice of coating materials, number of layers and thickness of layers depends on the end use of the product. Coating is a well-studied and well-established unit operation in numerous industries such as pharmaceuticals, paper and paperboard, wood products, steel, automobile, aviation, and packaging. Most coatings used in decorative and protective applications are solvent-based, the examples of which can be found in many ubiquitous products, such as wall paints, furniture, and vehicles. On the other hand, water-based coatings can be found in certain products like medicinal tablets, paper cups and packages, books, magazines, etc.

Due to environmental concerns related to solvent-based coatings, there has been an inclination in the coatings industry towards the utilization of more eco-friendly, renewable, and biodegradable materials. This trend has resulted in research efforts in three directions: (i) replacement of the harmful solvents with water or other environmentally benign solvents; (ii) use of bio-based coating materials; and (iii) integration of coated products in the circular economy. An example of this trend can be observed in the food packaging industry, which is under immense pressure to replace petroleum-derived plastic materials with biodegradable and renewably-sourced ones. As a result of efforts in the previous two decades, packaging researchers have identified many bio-based solutions suitable for replacing fossil-based plastic layers in food packaging. These solutions include water-based dispersion coatings, drop-in biopolymer coatings, biocomposite and bionanocomposite coatings, etc. [1]–[6]. Among these solutions, a material of special interest is nanocellulose, which has become an extremely popular research topic in recent times.

Apart from packaging, exciting applications of nanocellulose have been reported in literature in a wide array of technological fields, such as electronics, pharmaceuticals, cosmetics, and biomedicine. Some specific examples of these applications are in flexible energy storage devices [6]–[8], drug delivery systems [9], [10], tissue engineering platforms [11]–[13], water purification assemblies [14]–[16], etc. During the past decade, numerous novel nanocellulose applications have come to the fore, and the spectrum is widening at an astonishing rate.

2.1 Production and classification of nanocellulose

Nanocellulosic materials can be derived from various natural cellulose-containing sources such as plants, trees, bacteria, algae, wastewater sludge, and tunicates. These materials can be broadly classified into three categories on the basis of their morphology and production method viz. (i) cellulose nanofibrils (CNFs), (ii) cellulose nanocrystals (CNCs), and (iii) Bacterial nanocellulose (BNC). Nanocellulosic materials often appear in literature with different names such as

microcrystalline cellulose (MCC), microfibrillar cellulose (MFC), cellulose microfibrils (CMFs), nanocrystalline cellulose (NCC), nanofibrillar cellulose (NFC), etc. Figure 1 summarizes the classification and also brings together the parallel nomenclature of the same materials by different research groups. [17]

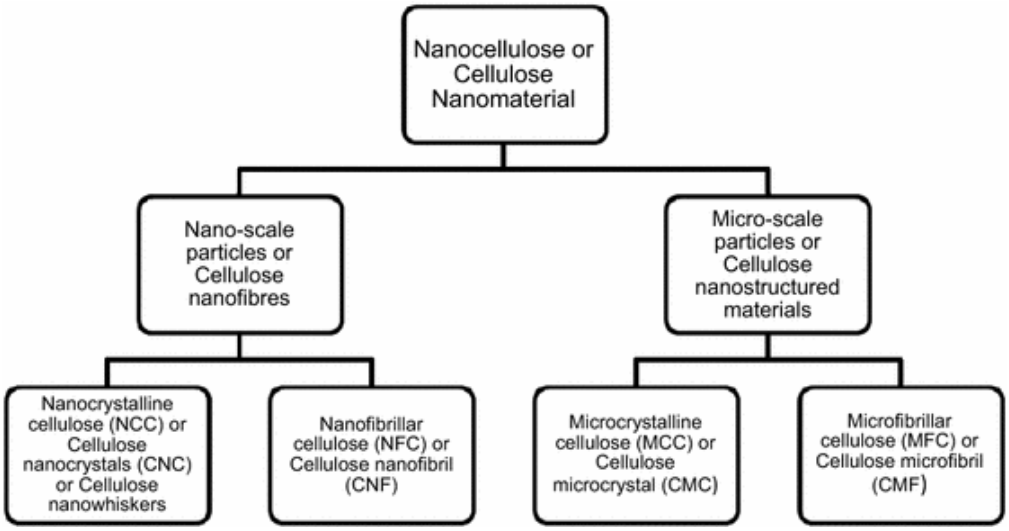

Figure 1: Classification of nanocellulose materials [17]

A number of techniques, roughly categorised into top-down and bottom-up approaches, have been developed to produce nanocellulosic materials. Here, the top-down approach means inducing cellulosic materials to mechanical and/or chemical action to obtain micro or nanofibrils, and the bottom-up approach denotes the use of special bacteria or algae to produce nanocellulose.

In the top-down approach (see Figure 2), extraction of nanocellulose from the source cellulosic material consists of multiple processes such as, chemical or enzymatic pre-treatment, mechanical treatment, acid hydrolysis, etc. In general, the pre-treatment operation involves any enzymatic or chemical treatment of the raw material in order to prepare it for further processing. For instance, while using wood as the cellulosic raw material, pulping and bleaching can be considered as pre-treatment steps. However, a majority of large-scale production facilities for fibrillated cellulose use wood pulp as the raw material. In this context, apart from purification and homogenization of the raw material, the pre-treatment step can also be utilized to impart surface charge to the fibers, which contributes towards the stability of the fiber suspension through electrostatic repulsions. A number of pre-treatments have been explored in order to increase the charge content on fiber surface such as, 2,2,6,6,-tetramethylpiperidine-1-oxyl radical (TEMPO)-mediated oxidation [18], carboxymethylation [19], carboxylation via periodate chlorite oxidation [20], sulphonation [21], and cationization [22]. Additionally, it has been shown that pre-treatment operation reduces the energy consumption in the subsequent refining operation [23], [24].

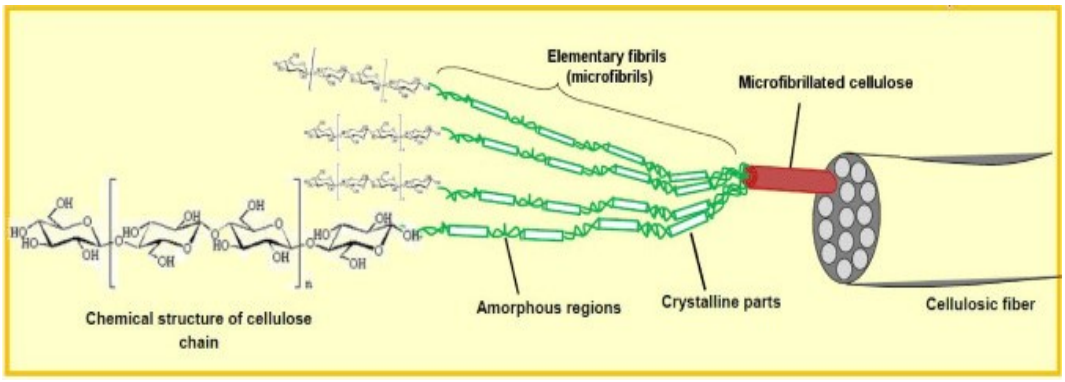

Figure 2: Schematic of nanocellulose extraction adapted from Lavoine et al. [25]

The second unit operation involves breaking down the cellulose material into nanoparticles using high-shear mechanical treatment. Typically, when pre-treatment is followed by mechanical treatment, the resulting nanoparticles are called cellulose nanofibril (CNF). Whereas, when cellulosic raw material is subjected to only mechanical treatment, a coarse grade material called microfibrillated cellulose (MFC) is obtained [26]. Another method to extract nanoparticles from cellulosic raw materials is acid hydrolysis, where using strong acids such as sulphuric, hydrochloric and phosphoric acid followed by dialysis, results in suspensions of cellulose nanocrystal (CNC). CNCs are rod-like, low aspect ratio particles while MFCs and CNFs are high aspect ratio fibrillar materials. The reason behind the difference in grades of nanocellulose via these two de-structuring routes lies in the inherent nature of cellulosic raw materials, which consist of both amorphous and crystalline regions. The disordered (amorphous) regions are preferentially dissolved during the strong acid treatment, leaving behind the more resistant crystalline regions.

These nanocellulose production processes are however energy intensive and are limited to production of low consistency aqueous suspensions. The high viscosity and yield stress of nanocellulose suspensions, even at low solids, makes the passage of high consistency suspensions through the grinding and homogenizing equipment rather difficult, and the efficiency of the defibrillation process is also hampered. Therefore, optimization of top-down technologies is needed, in order to reduce energy demand and production costs and to improve process yield and product quality.

On the other hand, in the bottom-up approach, cellulose producing bacteria such as *Acetobacter xylinum* are used to obtain nanocellulose fibers. Bacteria produce cellulose for possible reasons like protection from the environment and gaining access to oxygen [27]. Chemical constitution of BNC is the same as plant-based cellulose, however, it is free from secondary compounds, such as lignin, hemicelluloses, and pectin. The purity of BNC makes it very attractive for medical applications such as bone tissue regeneration, making artificial skin, wound dressing materials, etc.

Morphology-wise, BNCs typically form ribbon-like bundles with length in the range1-9 μm and diameter of 20-100 nm. Whereas, CNF have a diameter of 3-100

nm and length of up to 100 µm and usually form spaghetti-like bundles. Unlike BNC and CNF, CNCs have rod-like shape and usually, their length varies from 100 nm to several microns and diameter from 3-50 nm as per ISO/TS 20477:2017 definitions [25], [28]. Since the dimensions of CNC, BNC, and fine grades of CNF are smaller than the wavelength of visible light, diffraction effect causes the appearance of their suspensions to be transparent or translucent, whereas suspensions of coarse grades of CNF and MFC are typically opaque.

2.2 Nanocellulose in films and coatings

Cellulose fibers possess the ability to form intermolecular hydrogen bonds due to the presence of carboxyl and hydroxyl groups on their surface. Papermaking chemistry states that upon the evaporation of water in aqueous suspensions of cellulose fibers, the fibers come close together to form a strongly bonded paper network. The same principle applies to nanocellulosic materials, which undergo self-assembly upon drying. Hence, a controlled self-assembly procedure can be utilized to produce thin films and coatings from nanocellulose. Such films have been produced and investigated by a large number of research groups over the last fifteen years and have been reported to be transparent, mechanically strong, and to possess excellent barrier properties against oil, grease, and oxygen. Comprehensive reviews discussing nanocellulose films and their properties enlist the tremendous potential that the material possesses [26]–[28].

The mechanical properties of nanocellulose films depend greatly on the extent of intermolecular hydrogen bonding in the dry film. In turn, hydrogen bonding depends on many variables such as cellulose source composition, nanocellulose production method, fiber morphology, moisture, etc. An important parameter for fibrillar nanocellulose is the degree of fibrillation. Higher extent of fibrillation results in finer fibrils possessing large specific surface area and hence, offering the scope for more effective hydrogen bonding and surface functionalization. This effect can be observed from the transparency of CNF films. Since these materials possess large surface area due to small fiber size, extensive hydrogen boding leads to the formation of closely packed film structures. This causes minimal backscattering of light from fiber-air interfaces in the films, making them transparent with high clarity. On the other hand, films formed from MFC, while being transparent, usually have high haze because the film network is not as densely packed as in CNF films. The relatively larger fibril size of MFC also contributes to the light scattering. Additionally, CNF films are mechanically stronger than MFC films due to superior hydrogen bonding [32]. Transparency of CNC films can be explained using the same principle. However, pure CNC films tend to be brittle and the use of plasticizers, such as glycerol and sorbitol, has been reported in literature to reduce the brittleness [33], [34], [35].

Barrier properties of films are dependent on the tortuosity and compactness of the network structure formed due to the self-assembly of fibrils [36]. Due to the small size of nanocellulose, their dry films are densely packed and tortuous, thus not allowing fluids like oxygen, heptane, mineral oils, etc. to permeate through the film rapidly. However, due to the hydrophilic nature of the cellulose molecule, the dry film structure swells and becomes open upon contact with water or moisture.

Therefore, nanocellulose films as such are not able to demonstrate good barrier properties in high humidity environment. Many research groups have demonstrated treatment methods to improve the water vapour barrier of nanocellulose films. Few examples of such methods are coating native films with polymers such as LDPE, PLA, etc. or with beeswax, paraffin and starch [37].

Apart from standalone films, nanocellulose coatings have also been widely studied for applications related to barrier performance improvement of the base paper, improved printability, and surface functionalization. Among these applications, barrier improvement has been the most extensively targeted one with early publications reporting drastic drops in air permeance and improvement in oil barrier, due to the application of thin coatings on greaseproof paper [36], [38]. These findings were soon followed by studies reporting the improvement in surface strength, smoothness and bending stiffness offered by nanocellulose coatings [25], [38]. Studies on printing on smooth nanocellulose coated surfaces were reported by Song et al. [39] who found that the amount of dusting reduces during offset printing when a thin nanocellulose layer is applied on newsprint grade paper. Hamada et al. [40] reported the improvement in print quality when printing on a nanocellulose coated substrate with an inkjet process. A large fraction of literature deals with nanocellulose coatings in batch scale using a range of methods like rod coating with a drawdown coater, dip coating, spin coating, foam coating, spray coating, etc. Recently, use of continuous coating methods have been reported by Kumar et al. [41] and Koppolu et al. [42] where they demonstrated the use of slot-die for coating nanocellulose on paperboard.

2.3 Film thickness measurement

Quality control is an integral part of any commercial production process. Similarly, in coating processes, ensuring good quality of coating is important from both economic and sustainability perspectives. Here, coating quality is a qualitative parameter which is a resultant function of multiple factors such as uniformity in thickness, absence of defects, optimal coat weight application, drying strategy etc. One single parameter is seldom used to describe the coating quality since multiple variables are associated with the final quality in the process. Before commercial production starts, studies on substrate properties and coating formulation development are often concluded on laboratory scale. Optimal coat weight, which is usually related to coating thickness during processing, is also pre-selected based on the performance requirement of the coating. Modern coating processes possess the ability to control the final coating characteristics very precisely and the control is not limited to the metering element but also includes drying. The reasons for the need to precisely control a coating process include:

(i) saving material through the application of minimum sufficient coat weight
(ii) ensuring energy savings through the optimal use of drying capacity
(iii) monetary benefit through the use of lower amounts of materials
(iv) ensuring defect-free end product

(v) ability to modify the running process as and when needed

The scope of drying has been left out of discussion in the current work and emphasis has been paid towards the role of the metering unit operation for the final film thickness.

The coating industry has been utilizing various methods for online monitoring of coating thickness and/or coat weights in the past. The measurement techniques can be broadly classified into two categories, viz. contact and non-contact techniques. Both contact and non-contact testing methods have their advantages and disadvantages. Contact tests make direct physical measurements of sample dimensions and give the actual thickness value. However, the accuracy of such devices can be hampered when measuring small thicknesses on the sub-micrometer level. Apart from its physical limitations, contact testing finds itself unfit for applications in continuous roll-to-roll processes due to the nature of the test being destructive for coatings. On the other hand, non-contact testing does not touch the coating physically. This mode of testing relies on measurements of certain physical or chemical properties of the sample and relates them indirectly with the sample thickness. Non-contact testing is a more suitable approach for implementation in continuous processes due to its negligible interference with the sample. The sensitivity of such instruments can be controlled through the hardware while the performance of the device is tunable via the evaluation algorithm. However, these benefits are conjoined with high investment and maintenance costs, and the complexity of the devices often requires special training for machine operators.

Since the present work focuses on online measurement techniques and those are generally of non-contact nature, the subsequent text will deal only with non-contact measurement methods.

2.3.1 Non-contact techniques

There are numerous non-contact techniques, which have been demonstrated to measure thickness of thin films and coatings. Although many of these devices have been tested only in lab-scale batch processes, the possibility for upscaling to an online system has often been claimed. The classification of such systems into different types can be made on the basis of principle of operation. For instance, some prevalent industrial systems can be classified into electrical, magnetic, acoustic, and optical methods [43], and some of those are described below.

Electrical and magnetic methods

Capacitive sensing

Capacitive sensors were one of the first sensors to be utilized in the paper industry to measure the moisture content of the paper web. Their applications have not been limited to the paper industry, but they can be found in modern process plants as well as in automobiles, electronic gadgets, etc. The operating principle of capacitors is well-known and states that electrical energy is stored in the form of charge build up on electrodes, which are separated by a dielectric medium and observe a voltage differential.

Capacitance, an electrical property of capacitors, is a measure of the amount of charge that a capacitor can hold at a given voltage. Therefore, capacitance is defined as:

$$C = \frac{Q}{V}$$

where

C is the capacitance (in Farad),

Q is the magnitude of charge stored on each electrode (in Coulomb), and

V is the applied voltage (in Volts).

The geometry of a capacitor defines its capacity to store charge and hence defines its capacitance. Common types of capacitor geometries are parallel-plate, cylindrical tube, rod, and hexagonal with each type having its own specialized applications. For instance, cylindrical and tube-type capacitors are used for sensing liquid level in tanks, in brake fluid monitoring, tilt sensing, etc. [44]

Online capacitive thickness measurement systems can be either single-sided or double-sided, according to the requirements and the characteristics of the process. Both arrangements might use the same or different measurement principles. Typically, for one-sided thickness and proximity sensing applications, fringe-type capacitors are used. On the other hand, two-sided systems use either parallel-plate or fringe-type capacitors [45] (see Figure 3).

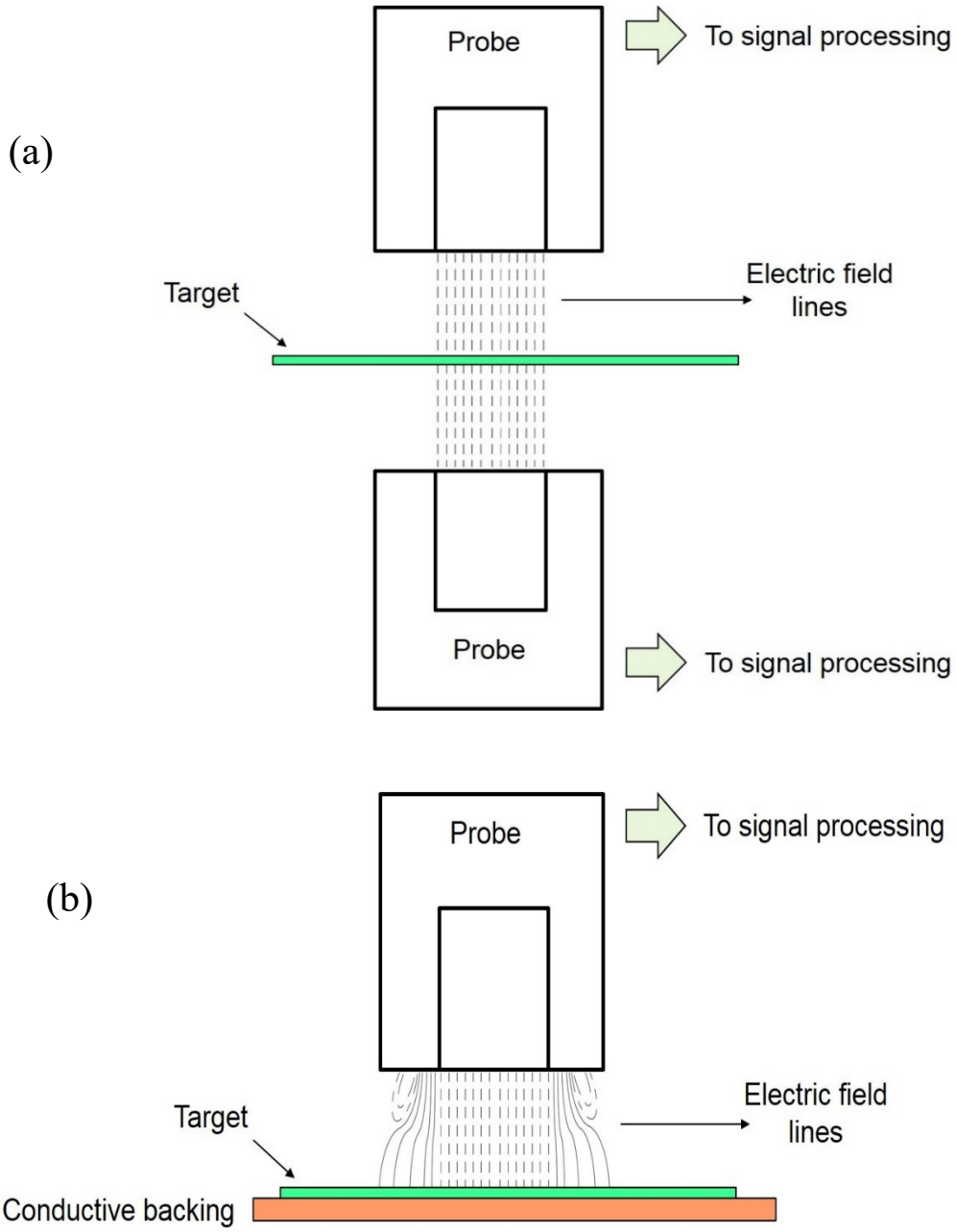

Figure 3: (a) Schematic of double-sided capacitive measurement using parallel-plate assembly and (b) single-sided measurement using a conductive backing

The parallel-plate capacitor model for measuring web thickness has a fixed requirement of being double-sided, since the electric field originating from the positively charged electrode passes through the target to meet the other electrode. In this case, the non-conductive target material acts as a dielectric medium, which lowers the intensity of the electric field passing through itself. The capacitance of a parallel-plate capacitor with a dielectric medium separating the two electrodes is calculated as:

$$C = \varepsilon_0 k \frac{A}{d}$$

where

ε_0 is the permittivity of free space (vacuum), equal to 8.854 x 10^{-12} F/m,

k is the dielectric constant of the medium, also known as relative permittivity,

A is the area of capacitor plate, and

d is the distance between the plates.

Using the above equation, the dielectric constant of a dry film can be determined by measuring the capacitance of a film of known thickness. This is a typical calibration step and is subsequently followed the actual measurement where the capacitance is a function of only the separation between the plates. For contactless measurement, in order to compensate for the change in the dielectric constant due to the presence of air between the electrodes, the multiple dielectric media model is used. In this model, the capacitance between each parallel surface lying within the capacitor plate gap, is added in series to obtain a total capacitance as follows:

$$\frac{1}{C_{total}} = \frac{1}{C_1} + \frac{1}{C_2} + \cdots + \frac{1}{C_n}$$

where

C_{total} is the total capacitance of the system.

C_1, $C_2 \ldots$ C_n are the individual capacitances between parallel surfaces within the capacitor plate gap, e.g., capacitance between the electrode and the dielectric surface, capacitance within the dielectric medium, etc.

However, the actual observed capacitance of a parallel-plate capacitor is always more than the theoretically calculated value. The extra capacitance is called fringe capacitance, which is generated due to non-linear electric field originating at the edges of the electrode plates. For some applications, solely the fringe capacitance is utilized for measurements. But even in this case, the measurement principle, nonetheless, remains the same with the non-conductive target acting as a dielectric to the capacitor and the change in capacitance being a function of the dielectric thickness.

Both single-sided and double-sided measurement assemblies are used in the industry, with each having its own advantages and disadvantages. An advantage of using a double-sided system is that the results are not affected by web flutter. The parallel-plate model also works over a larger probe-to-target distance, as compared to fringe capacitance method. However, single-sided instruments are more popular capacitive measurement systems for measuring dielectric and insulating materials like plastic films and paper. Since most web-based processes utilize rollers, it is convenient to place a single-sided device on a portion of the web supported by a conductive idle roll. The placement of probes on top of a roll removes the impact of web flutter but might add error to the measurement through machining flaws in

the backing roll. Additionally, with time and wear, the backing roll might become eccentric causing the target to lose its parallelity to the probe.

A major limitation of capacitive measurement methods is the loss of accuracy upon increasing distance of the probes from the target. Authors have shown that the output signal starts to lose its linearity when the probes are placed more than 1 mm away from the target [45], [46]. Therefore, the probes have to be placed close to the target, which might not be possible in all kinds of online applications as the size of probes might become too big for larger measurement distances. Also, temperature and humidity affect the dielectric constants of materials. Although modern sensors are housed in robust casings, the sensor installation position has to be selected carefully to keep the calculation parameters constant. In the case of fringe capacitance method, the measurement probes must be guarded against stray capacitance and noise, since the output signal is much weaker as compared to the parallel-plate method.

Capacitive sensor technology is quite mature, inexpensive, and reliable. Additionally, the absence of mechanical parts and contactless operation of these systems allow them to have a long functional life. Their compact size and light weight also allows installation on small pilot machines. Although these devices can be tuned by changing the probe type, their operating range is not very flexible. Currently available parallel-plate devices in the market claim a nominal range between 25-800 μm. The maximum limit is improved by using cylindrical capacitors to up to 2000 μm, but the lower limit is not affected much. As a result, the measurement range of capacitive devices is limited on the lower end of the range. Typically, the dry film thickness of nanocellulose coatings is much lower than the lower limit of capacitive devices and hence, such devices can only be used for wet coating layer measurements. Homogeneity of the film material is also a critical factor in such measurements, since the electrical properties of materials vary with a change in solids content, amount of additives, presence of lumps, entrapped air, etc. Therefore, it can be concluded that although capacitive sensing has its advantages, it is not the best available technology for online measurement of nanocellulose films and coatings. There is often a need to combine the technique with inductive sensing to produce higher precision.

Inductive sensing

Inductive sensing technology works on observing changes in the magnetic field produced by the inductor present in sensor probes when brought in the proximity of a target. Several techniques using inductance based devices exist, and the mode of operation of sensors varies depending on the magnetic characteristics of the target and backing material (if present).

One approach of using inductive thickness gauges is the direct measurement of the change in magnetic field strength upon interaction with a target. The strength of the magnetic field depends on the permeability of the propagation medium. Calculation models for non-magnetic targets placed on top of magnetic substrates can be built

when the excitation parameters are known. This approach usually uses excitation current to produce a low-frequency magnetic field which penetrates the non-magnetic target, as shown in Figure 4. Industrially, this technique is used to measure the thickness of paint, enamel, plastic coatings, and electroplated layers of chromium, zinc, copper, aluminium, etc. on steel and iron [47]. However, the measurement range of this method is limited to low thicknesses, typically less than 200 µm [45]. Also, accurate measurements require a very small lift-off from the target, usually less than 1 mm [48] and in some cases, measurements might not be possible without ensuring physical contact between the probe and the coating. This approach is not feasible for industrial use in regard to nanocellulose films and coatings for two reasons- (i) the wet film thickness (WFT) is usually much higher than the measurement range of the devices, and (ii) contact measurement would be required on the dry-end, which is not practical for high-speed operations.

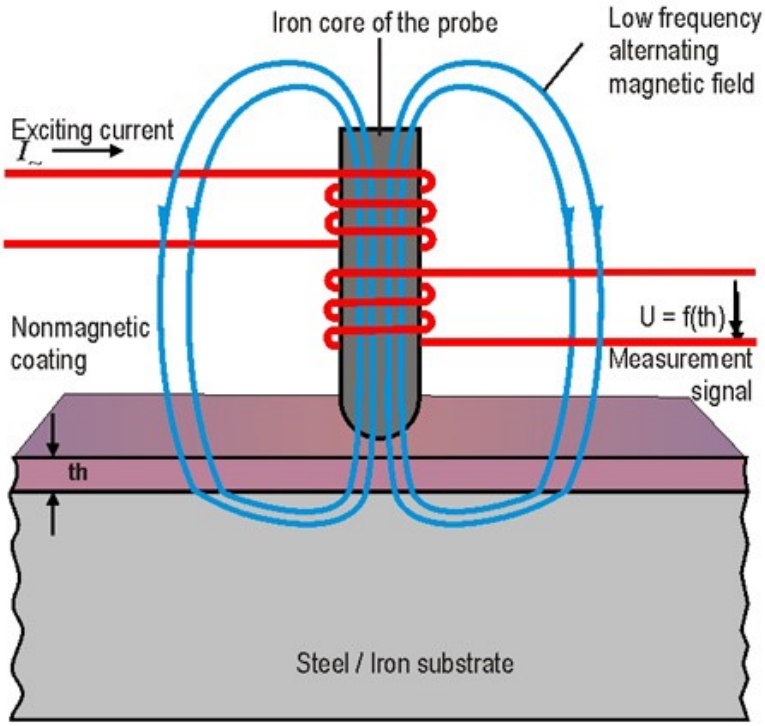

Figure 4: Schematic of a direct inductive sensor [47]

The second approach used in inductive sensing devices is based on the generation of eddy currents in the target material. The core principle behind eddy current based inductive sensing is Faraday's law of electromagnetic induction, which states that the induced electromotive force (EMF) in a circuit due to a change in magnetic flux is equal to the rate of change of the magnetic flux through the circuit. Faraday's law explains the concepts of self-induction and mutual induction, where the latter is used by sensing instruments. Mutual induction is the phenomena where an EMF is produced in a circuit due to a change in the current in an adjacent circuit which is linked to the first by magnetic field lines. Thus, a sensing probe containing a coil can interact with a conductive target through the magnetic field produced upon the passage of current through the coil.

Through this magnetic interaction, eddy currents are produced in conductive targets, which in turn, produce their own magnetic field to oppose the excitation field. Since the eddy current density depends on the distance between the probe and the conductive surface, the strength of the opposing magnetic field also depends on the distance. High-frequency magnetic field, typically several hundred Hertz, is used in this approach in order to produce sufficiently strong effect of eddy currents on the output signal and to allow a high signal-to-noise ratio (SNR) [49], [50].

The eddy current approach can be used only in special cases where the film material is both non-conductive and non-magnetic, while the substrate is an electrically conductive non-ferrous metal. Such combinations of film and substrate can, for instance, be found in paints on aluminium, copper and certain grades of stainless steel, such as 316 and 316L. In regard to nanocellulose film casting on steel belts, this method can prove to be useful. However, such limited applicability of these devices reduces their appeal for more established usage. Akin to the direct inductive sensors, eddy current sensors also work with small lift-offs and are unable to measure thick films. These both drawbacks make them unsuitable for measuring thick wet layers of nanocellulosic materials. However, eddy current sensors are suitable for use at the dry-end of coating machines since they do not necessarily require contact and are able to measure non-magnetic non-conductive thicknesses in the range of 2-100 μm [50]–[52].

Inductive sensing technology is widely used for proximity, position, and thickness sensing in the automobile and metal processing industries. Its use has also been prevalent in the food industry for measuring varnishes and in the electronics industry for measuring the thickness of LCDs [53]. However, due to its operating principle being dependent on electrical and magnetic properties, inductive sensing technology is limited by the types of targets that it can be applied for. Even if conductive backing rolls are used behind non-conductive substrates, the cumulative thickness of the film and the substrate is enough to significantly hamper the measurement. However, as the applications of nanocellulosic materials are growing rapidly, the substrates for coatings are also changing and will not be limited to fiber-based materials. For instance, metal and glass have been explored recently as substrates [54]. Therefore, eddy current based inductive sensing holds potential to be applied for online measurement thickness of nanocellulose films and coatings on conductive substrates, especially on metals.

Optical methods

Spectroscopy

Spectroscopy is a broad term which covers a wide range of techniques that work on the principle of observing the interaction of electromagnetic radiation with matter. Since different regions of the electromagnetic spectrum possess different attributes, modern spectroscopic devices are able to exploit a wide range of the spectrum, such as, ultraviolet (UV), visible, microwave, and infrared (IR) [55]. Among these, IR spectroscopy is by far the most frequently used technology for coating analysis [56]–[58]. It is fairly old and well-studied technique for identification of molecules though its utilization for film thickness measurement is comparatively new, with first uses coming into the fore in the 1990s in the semiconductor industry [59], [60].

The IR spectrum can be divided into three regions based on wavelength (or wavenumber), namely, far-IR (400-0 cm^{-1}), mid-IR (4000-400 cm^{-1}), and near-IR (14285-4000 cm^{-1}). Majority of commercial instruments employ only the mid-IR and near-IR (NIR) wavelengths for operation, given the relevance of these two spectrums to most molecules. IR spectrometers also possess the ability to operate in either transmission or reflectance mode (see Figure 5). Ultimately, the choice of the measurement mode and the sweeping wavelength range depend on both chemical and physical attributes of the sample. The testing hardware and sample preparation methodology varies with sample characteristics.

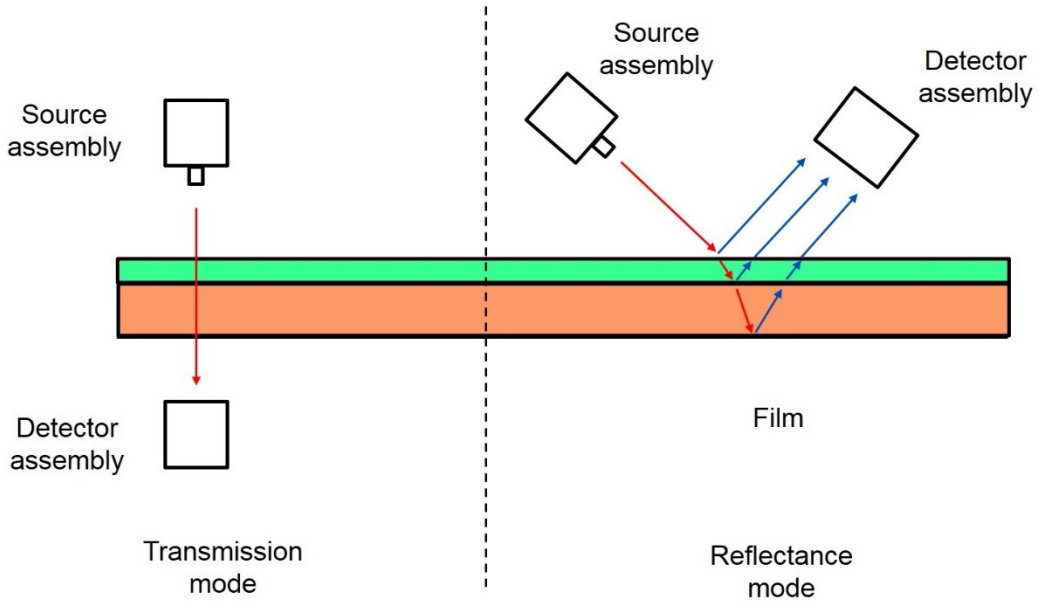

Figure 5: Schematic of measurement geometry in IR spectroscopic devices, using transmission mode (left) and reflectance mode (right)

IR spectroscopy is a technique based on the absorption of incident energy due to vibration of atoms in molecules. A molecule absorbs radiation when the frequency of the incident radiation is the same as the frequency of one of the fundamental modes of vibration of the molecule. Here, the fundamental modes of vibrations are

defined in terms of stretching, bending, or rotation of bonds between atoms. Upon interaction with incident IR radiation of varying wavelengths, molecules exhibit a spectrum, which is devoid of a fraction of energy at certain wavelengths, due to absorption. The characteristic vibrations for which an IR spectrum exhibits absorbance peaks is an intrinsic property of molecules present in the sample, and the spectrum can hence be utilized for chemical composition analysis using reference spectra. Additionally, a higher concentration of a certain species in a sample causes more absorbance of energy at the species' corresponding wavelengths. This phenomenon can be expressed numerically using the Beer-Lambert law, which states the following:

$$A = \log\frac{I_0}{I} = a.c.l$$

where

A= Absorbance, I_0= Intensity of incident light, I= Intensity of emerging light, a = absorptivity coefficient, c = concentration of absorbing species, and l = optical path length.

According to the abovementioned equation, if the target film has a homogenous composition, by measuring the absorption of the incident radiation and by experimentally determining the absorptivity coefficient, the thickness of the homogenous film can be calculated. However, Beer-Lambert law is a linear approximation of a more complex relationship between absorbance of light at a particular wavelength to the concentration and optical path length and therefore, corrections are applied to the basic law, depending on the sample properties. For instance, the linear proportionality of absorbance with concentration is valid only for low concentrations, typically in the order of 0.01 M [55]. In addition, this equation considers a plane-parallel model for calculation, whereas for practical purposes, measurements might be performed at a certain angle to the target surface. Tolstoy et al. [61] described the governing equations that represent the physics in different modes and geometries of IR spectroscopy.

IR transmission spectroscopy uses the principle of Beer-Lambert law and is a comparatively simpler film analysis method as compared to reflectance methods. For precise chemical analysis purposes, liquid samples are usually measured in special solution cells. Solids can be either dissolved in a solvent and put in solution cells or can be mixed with alkali halides and formed into clear tablets. On the other hand, for film thickness measurement purpose, the absorption spectrum of the substrate, with and without the film is measured and subsequently, the substrate spectrum is subtracted, leaving behind the pure film spectrum.

However, using the transmission mode for online measurements demands certain properties from both film and substrate. Both materials must be optically thin, i.e. should allow sufficient radiation to pass through them and be detected on the other side. Since the substrate is usually much thicker than the dry film, it occupies a large fraction of the maximum permissible optical path length and this already puts an upper cap on the measurable film thickness through this method. Thin polymer

films, up to 50 µm are measured comfortably with this method when the thickness of the substrate is roughly 1 mm [62]. But this range is highly dependent on the optical properties of the target material. For instance, the presence of IR radiation absorbing or highly reflective materials greatly reduces the SNR in the measurement. Also, non-metallic substrates are particularly susceptible to variations in optical properties [63]. Apart from these problems, installing double-sided spectrometers in an online system is itself a challenge. To overcome such challenges, reflectance-based methods are adopted.

IR spectroscopy is used in the reflectance mode for analysing samples which exhibit high reflectivity and are generally not characterizable in transmission mode. Reflectance mode also allows single-sided measurement, which is a major advantage of this method. There are two major approaches, which can be employed in the reflectance mode for measuring film thickness, namely, absorption method and optical interference method. Theoretically, both interference and absorption have influence on the output spectrum but for simplicity of measurements, only the output generated due to the dominating effect is taken into account in older instruments. However, in cases when both effects contribute significantly to the output signal, neither one can be neglected [62].

Absorption method in reflectance mode also works on the same principle as in the transmission mode, where the reduction in radiation intensity upon interaction with the sample is correlated to parameters such as optical path length, refractive index, absorptivity coefficient, and wavelength of incident light. Upon fixing variables through instrument design and calibration, a mathematical relation between absorbance and film thickness can be derived [61], [62], [64].

On the other hand, the interference method in reflectance mode works on the principle of observing the interference of light rays reflected from the top and bottom surfaces of the target film. A light ray reflected from the bottom surface travels a longer path to reach the detector than a ray reflected from the top surface. This difference in path length creates a phase difference between the two rays. Rays in phase with each other create a constructive interference and the ones out of phase cause a destructive interference. The intensity of the output signal is thus dependent on the interference of the two reflected rays, which is in turn, dependent on the thickness of the film. Several authors have studied this method of film thickness measurement in recent times and reported improved correlation techniques for error elimination [65], [66] as well as novel measurement setups [57].

Due to their high cost and complexity, most spectroscopic techniques, such as photoacoustic, attenuated total reflectance (ATR) [67], laser-induced breakdown, [68], terahertz spectroscopy [69], [70] etc. have seen limited usage for film thickness measurements. However, these techniques have been utilized for precise measurement of thicknesses in the nanometer range, e.g. in atomic layer deposition (ALD) or chemical vapour deposition (CVD) processes. Whereas, simpler, inexpensive and rapid techniques like NIR absorbance spectroscopy have seen a much wider use in measurement of thicknesses in the micrometer range, upto several hundred micrometers. For instance, such devices are used in the

pharmaceutical industry to monitor thickness of tablet coatings and polymer films. In the paper and board industry, NIR method is used to determine moisture level in the web.

In spite of its benefits, a major disadvantage of IR absorbance method is that measurements are limited to a certain maximum thickness, depending on the target material due to the 'disappearance' of the substrate in the output spectrum. The disappearance of substrate happens due to excessive absorption of incident radiation by highly concentrated film components, leaving the absorption peaks from the substrate relatively insignificant. This problem is especially notable for water-based coatings, which are applied in the form of dilute suspensions, like in case of nanocellulosic materials. Since nanocellulose film suspensions are very dilute (typically, 0.1-3% solids), devices essentially measure the thickness of a pure water film on the substrate. Water is a strong absorber of IR radiation and hence provides a strong response to the measurement system. But as the water film thickness increases, a large fraction of the incident radiation begins to be absorbed by water molecules and a limit is reached after which the device signal no longer remains sensitive to increasing layer thickness [69].

As a conclusion, spectroscopic methods prove to be versatile and powerful tools for thickness measurement of thin-films, even in the nanometer range, for offline applications. However, for online applications, their utility is limited to films less than 100 μm thick. Typically, for water-based films, measurements can be made for thicknesses up to 500 μm but a practical limit arises for films thicker than that. Improved evaluation algorithms for processing spectrum data are possible to be developed, but those might hinder the measurement speed and still not be valid for thicknesses in the range of 1000 μm. However, their performance within their measurement range is excellent in terms of accuracy, precision, and repeatability, making them very relevant for industrial use.

Thermography

Every object possessing temperature more than absolute zero radiates energy in the form of electromagnetic radiation. This radiation contains a range of different frequencies and hence creates a spectrum where every radiation spectrum possesses a peak at a certain characteristic frequency. The characteristic frequency depends on the temperature of the object, with higher temperatures producing higher characteristic frequencies. Planck's law of blackbody radiation describes this phenomenon mathematically as follows:

$$I(v,T) = \frac{2hv^3}{c^2} \times \frac{1}{e^{\frac{hv}{kT}} - 1}$$

where

$I(v,T)$ = Power per unit surface area per unit solid angle emitted at frequency v by a blackbody at temperature T, h = Planck's constant, c = speed of light, and k = Boltzmann's constant.

The abovementioned Planck's law can be integrated over the frequency domain to obtain a function for total emitted radiative power by a body. The integration results in yet another prominent relation known as the Stefan-Boltzmann law, which states the following:

$$P = A\varepsilon\sigma T^4$$

where P = total radiative power emitted by an object, A = radiative surface area, ε = emissivity, σ = Stefan-Boltzmann constant, and T is the surface temperature of the object.

For objects at low temperatures, the emitted radiation lies in the infrared region of the electromagnetic spectrum. Hence, human eyes are unable to observe radiation from everyday objects. However, bodies start to emit a significant amount of visible light as their temperature increases beyond approximately 500°C, causing human eyes to observe a 'glow' in hot objects. However, most coating processes seldom reach temperatures in the range of 500°C. Therefore, in order to utilize emitted radiation to measure coating process parameters, IR cameras are used to detect radiation and convert the signal into electronic form to generate images. This method of imaging objects based on their infrared radiation emission is called thermography.

Thermography is a widely used technique to study material characteristics, structure analysis, and non-destructive testing (NDT) in aerospace, automobile, construction, and metallurgy industry. Since thermographic methods detect radiation in the IR range of the electromagnetic spectrum, the technique is often called IR imaging or IR thermography (IRT). As an output, IRT produces images of objects based on their temperature. For instance, Figure 6 illustrates a thermographic image of a plastic web entering an oven in an online process, where the temperature difference is clearly noticeable. Apart from producing heat maps, images, and temperature profiles, thermographic methods can be used for detecting cracks in metals, glass, concrete, etc. Such cracks create local 'hot spots' that can be located using thermography and thus, structural failures can be prevented [71].

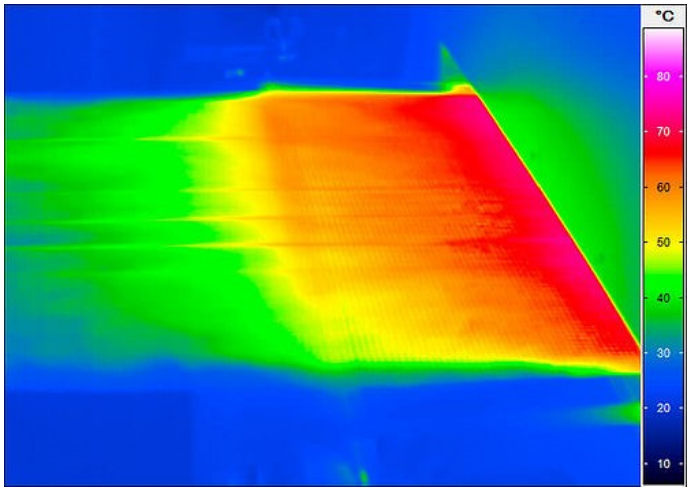

Figure 6: In-process image of a plastic film taken from an IR camera [72]

However, radiation from a target object might or might not be sufficient for producing a high SNR during thermographic measurements. SNR is affected by various factors like location of the measurement system in the process, ambient conditions, temperature of background objects, properties of target material, etc. Therefore, there is often a need to stimulate the measurement target by using external excitation. Many different methods have been demonstrated to stimulate targets externally, such as ultrasonic waves, microwave radiation, laser beams, IR radiation, eddy currents, etc. but IR radiation is the most commonly implemented method [73]–[77]. Many authors have reported mathematical techniques to diminish errors resulting from improper correlation between detected radiation and film thickness. Such errors might arise from conduction or convection effects, inaccurate measurement of thermal properties of targets, deviation from calculation model assumptions, etc. [78]–[81].

Thermographic techniques can be broadly divided into two categories, viz. active and passive thermography. Here, the basis of differentiation is that active methods stimulate target materials using external excitation while passive methods detect only the natural radiation from targets. Active methods are more commonly used because they allow the possibility to enhance signal quality and to control measurement conditions. Additionally, in active methods there can be multiple modes of external stimulation of targets such as short-pulsed, long-pulsed, lock-in, step heating, modulated, etc. [71], [82]. Describing the exact methodology of all the excitation modes is out of the scope of the current work, however, active lock-in infrared thermography is described in Materials and Methods section, since it was utilized in the current work. Some devices working on the same principle as IRT do not generate images but use the spectral data directly to measure target material characteristics, such as thermal effusivity, thermal diffusivity, thermal conductivity, heat capacity, etc. Such techniques are sometimes termed as photothermal detection techniques.

Typically, lab-scale active IRT techniques are able to measure film thickness ranging from 1-1000 μm [71], [83]. However, this range varies with targets that possess different thermal and optical properties. For instance, commercial devices from Erichsen GmbH and Winterthur Instruments AG are stated to have measuring ranges of 0-2000 μm for powder coatings on metals and polymer coatings on wood, glass, carbon fiber reinforced polymers (CFRP), etc. For these devices, the maximum web speed lies in the range of 50-120 m/min and maximum lift-off lies in the range of 5-20 cm. A major advantage of using IRT is its applicability to a wide selection of materials and a wide measurement range. Unlike spectroscopic techniques, the performance of IRT methods is independent of the chemical composition of targets and it gains an upper hand to electric and magnetic methods in terms of allowing a greater lift-off. A significant disadvantage of IRT is its high sensitivity to thermal and optical properties of target material, which might vary in the process. Additionally, improper calibration and calculations based on erroneous signal evaluation models might cause inaccuracy in the results. However, this might be due to the fact that the concept of utilizing IRT for measuring film thickness is rather new and patents have been granted for such devices only in the last decade [84], [85]. Apart from improvements in hardware, novel signal processing models

employing machine learning in addition to thermodynamic modelling [80], [81] have been reported recently. It can be concluded that this technique is being investigated and improved continuously, and it possesses great potential to become a powerful industrial technique in the future.

Laser and white-light displacement methods

The utilization of electromagnetic radiation for position sensing is commonplace in today's world, ranging from simple devices like automatic doors to sophisticated systems like RADAR. Precise position sensing, typically used for detecting displacement, has been utilized for measuring layer thickness since 1970s [86]. Such sensing devices operate either in the low-energy invisible or in the visible part of the spectrum and can be categorized into three types based on their mode of operation, viz. triangulation, optical interference, and chromatic aberration.

Triangulation is one of the most popular techniques to determine thickness of planar objects. It is essentially a geometrical technique that uses triangles to calculate distances. Specifically for surface location applications, triangulation requires measuring the deflection of a reflected beam upon change in position of the target [87]. Figure 7 illustrates a triangulation setup used by a commercial system manufactured by Keyence Inc. [88]

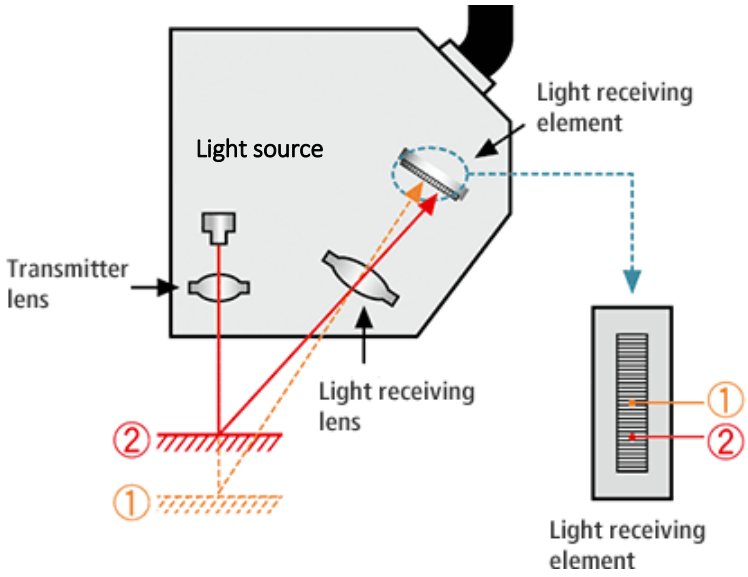

Figure 7: Schematic of a diffuse-reflectance triangulation system [88]

Triangulation devices can be used for thickness determination when the position of one surface of the sample is already known with sufficient accuracy. For instance, in case of web-based processes, the position of backing roll might be used as a reference for web thickness determination. In situations where a reference position cannot be determined, it is necessary to locate both surfaces of the sample simultaneously. This can be achieved by using a two-sided measurement system that also nullifies the effect of web movement in thickness dimension as an additional advantage [86]. Triangulation can be used reliably to measure thick webs, in the range of several hundred microns to tens of millimetres but to detect

smaller features, there is a need to use focused laser beams and special conditions. For instance, Khramov et al. [89] reported the minimum measurable thickness of plastic films using a 532 nm semiconductor laser to be 230 μm. Peterson et al. [87] reported that triangulation sensors could not take measurements from highly reflective surfaces due to excessive intensity of reflected light. Smith and Zheng [90] also studied measurement error introduced by sensor orientation and specular reflectance. Murakami [91] described the development of a novel calibration system using a laser interferometer which eliminated nonlinearity errors in laser triangulation sensor data. When dealing with multiple optical interfaces, e.g., in case of nanocellulose film casting on plastic substrate, correction for refraction effects must also be made. These corrections are well-known and have been derived from the Snell's law and basic geometry [92], [93].

The second type of sensors work on the principle of optical interference. Both white light and laser-based interference sensors work on the principle of interference of light waves, as described above under the spectroscopy heading. Interference-based techniques are primarily used in single-sided geometry for measuring thin transparent films, in the range of 2- 100 μm [94], [95]. However, such systems are expensive and high sensitivity of the method to refractive index and light interaction properties of film material makes it unsuitable for online thickness measurement. Consequently, even when the method is known for many decades, only a handful of commercial devices use it. On the contrary, the relatively new confocal chromatic method has come into the fore with major players in the sensors industry, such as Keyence, OMRON and Micro-Epsilon offering systems based on the method.

Chromatic confocal sensors work on the principle of chromatic aberration. Polychromatic light is passed through a series of lenses (see Figure 8), which split the light into different constituent wavelengths. These rays of light having different wavelengths focus at different focal planes, with longer wavelengths converging at a larger distance from the lens than short wavelength. Thus, a polychromatic focal line is created whose length defines the measurement range of the sensor. When the target is placed at a certain position in the focal line, the reflected signal observes a peak in the intensity of the wavelength that corresponds to the distance at which the target surface lies from the lens. Hence, the position of the light intensity peak in the reflected spectrum defines the distance between the lens (reference plane) and the target surface [96].

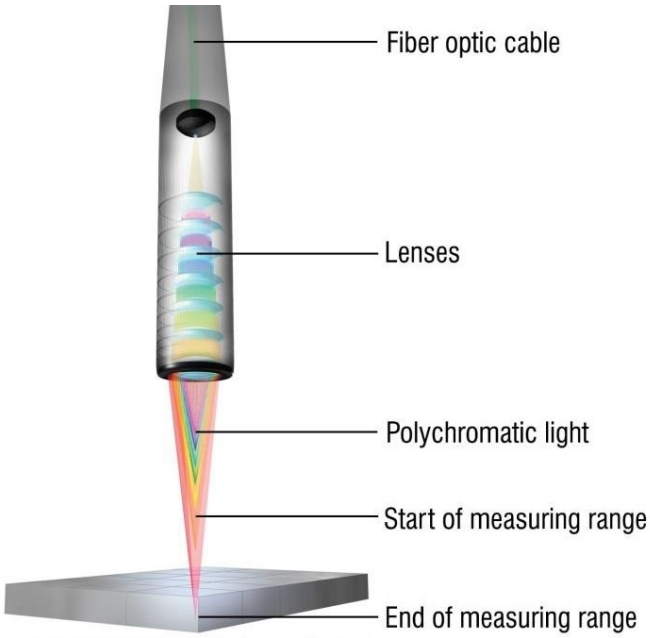

Figure 8: Schematic of an optical confocal system [97]

Optical confocal technique works on the principle of locating the physical surfaces of the sample and hence, measurements are not affected by the sample composition. Moreover, the measurement rate of optical systems is dependent only on the response rate of the used photodetectors. Modern systems allow measurement rates as high as 50 kHz, thus making them suitable for high-speed online processes. Such devices are also relatively inexpensive when compared to thermographic or spectroscopic systems. They are not affected by humidity, target conductivity or magnetization like capacitive and inductive sensors and they are immune to temperature and acoustic variations. They allow a large lift-off that makes their placement on machines convenient and keeps the sensors safe in case of web breaks. However, a major challenge in designing purely optical systems for thickness measurement lies in achieving adequate rigidity in the mechanical framework. These systems are highly susceptible to displacement and their operation is often realised as a compromise between thickness resolution and vibrational errors. In other words, a system designed for delivering high resolution observes a higher effect of vibrations.

Triangulation-based devices can potentially be an excellent choice for measuring thick low-reflectivity coatings on rigid substrates like metal, glass, ceramic, paperboard, etc. For smaller thicknesses and transparent films, interference-based devices are more useful. Confocal chromatic devices are most suitable for measuring translucent and opaque films, such as those of microfibrillated cellulose, in the range of 1- 2000 µm.

In order to assess the suitability of any technique for measuring thickness of nanocellulose films or coatings, performance requirements for techniques must be stated. Such requirements might vary based on end-use of the films, for example, a better accuracy might be required for applications in the electronics industry as compared to food packaging industry because tolerance for thickness variation is generally lower in the former. Since nanocellulose films and coatings, in the current state-of-the-art are prepared using suspensions having consistencies lower than 10%, a large amount of water is associated with suspensions. Thus, thick wet layers need to be deposited to get sufficiently thick dry layers. On one hand, the applied wet film thickness is beyond the measurement range of techniques such as, inductive sensing, beta-ray, and tomography. On the other hand, the low thickness of dry nanocellulose films could pose a challenge to techniques such as capacitive sensing. Techniques which offer a wide measurement range, are flexible with measurement geometry, and are accurate for a number of nanocellulose grades are suitable to be used for research purposes. Hence, in the current work, NIR spectroscopy, IR thermography and optical confocal displacement sensing were identified as techniques which fulfil the abovementioned requirements and were selected to be tested.

3. Materials and Methods

3.1 Materials

3.1.1 Film materials

The coating formulations used in the study were aqueous suspensions of nanocellulose fibers containing two additives viz. D-Sorbitol and polyvinyl alcohol (PVA). Two types of nanocellulosic materials were used, namely, MFC and CNF. The MFC was supplied by Borregaard (Exilva F 01-V) at 10% consistency and was dispersed in distilled water using a Minibatch Type 20 mixer (Diaf Pilvad Aps) to reach a consistency of 3%, before the addition of additives. The CNF was produced using TEMPO-oxidation of bleached Kraft pulp fibers and supplied by Empa, Switzerland and was supplied at 1.2% consistency. Both, MFC and CNF were delivered as aqueous suspensions and subsequently, all required dilutions were made using distilled water. D-Sorbitol was obtained from Sigma Aldrich, Finland Oy with more than 99% purity. PVA was procured from Kuraray Europe GmbH, Germany (trade name POVAL 6-98) with 98-98.8 mol% degree of hydrolysis. In total, two nanocellulosic formulations were developed and used throughout the study. Both formulations contained the same type and amount of additives but one formulation contained MFC and the other contained CNF. Table 2 shows the recipes, and Figure 9 shows the appearance of both formulations. In further discussion, the terms MFC and CNF denote the formulations based on the same materials respectively.

Table 2: Recipes for coating formulations for MFC (left) and CNF (right)

Component	Amount (pph)
MFC	100
D-sorbitol	20
PVA	10
Total solids (%)	**2**

Component	Amount (pph)
CNF	100
D-sorbitol	20
PVA	10
Total solids (%)	**1.5**

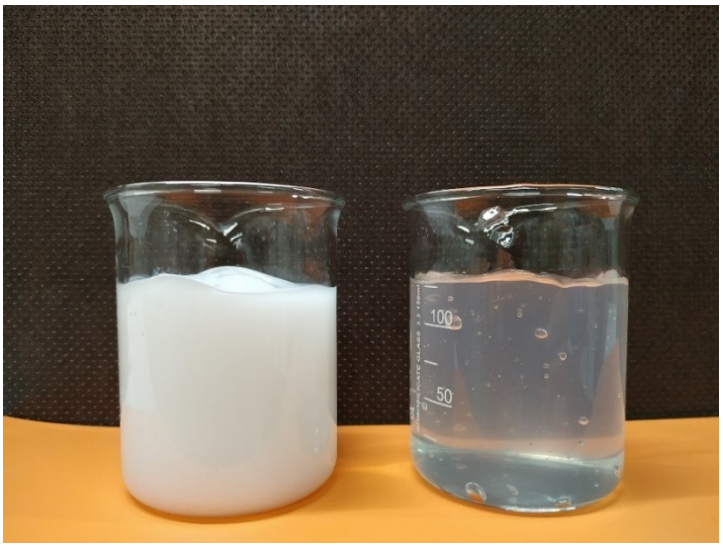

Figure 9: MFC (left) and CNF (right) formulations

3.1.2 Substrates

Three types of substrates were used in the study: a plastic, a polymer membrane, and a metal. The plastic substrate was chosen to be biaxially oriented polypropylene (BOPP) having a nominal thickness of 50 µm and was procured from Suomen Pakkausmateriaalit Oy, Finland. The polymer membrane used in the work was a commercial polyether sulfone (PES) membrane (nominal pore size: 0.8 µm, type: 15404) with thickness of 145 µm supplied by Sartorius Stedim Biotech GmbH, Germany. The metal substrate was selected to be a 1 mm thick (nominal) temper-rolled 304 stainless steel, obtained from Outokumpu Oyj, Finland, cut into A4 size sheets. The steel and the membrane were used for coatings directly but the plastic was treated with a plasma module (Vetaphone Corona Plus) while using a 2 kW generator and a mixture of argon and nitrogen gas in the 20:80 ratio.

3.2 Coating method

Laboratory coatings were made using a benchtop film applicator manufactured by Erichsen GmbH, Germany. The metering of the coatings was done using rigid knives supplied along with the coating device. The film application was performed at a constant draw speed of 3 m/min throughout the study for the ease of comparison of results. Three different knife gaps were chosen for lab-scale coatings viz., 700, 500, and 300 µm, in order to test the accuracy of the thickness measurement systems in a relevant range. A different set of knife gaps i.e. 700, 300, and 100 µm was used only in the case of NIR spectroscopic measurements in order to test the efficacy of the NIR system in measuring small thicknesses. The two variables: draw speed and knife gap, can be used to calculate the shear rate under the knife during film formation using the following equation:

$$\dot{\gamma} = \frac{v}{z}$$

where, $\dot{\gamma} = \text{shear rate } (1/\text{s})$, $v = \text{draw speed } (\text{m/s})$, $and\ z = \text{knife gap } (\text{m})$.

Since nanocellulose flow behaviour is highly dependent on the applied shear rate, fixing the draw speed and knife gap allows the shear rate under the knife to be constant for a given gap throughout the study. This allows easy comparison between samples created at different time, since the applied wet film thicknesses for the same gap does not vary theoretically. The schematic of the coating method is shown in Figure 10. After coating, the samples were dried in an oven at 80 °C for 20 minutes and then kept overnight in a climate controlled room at 23°C and 50% RH. Three parallel samples of each type were prepared.

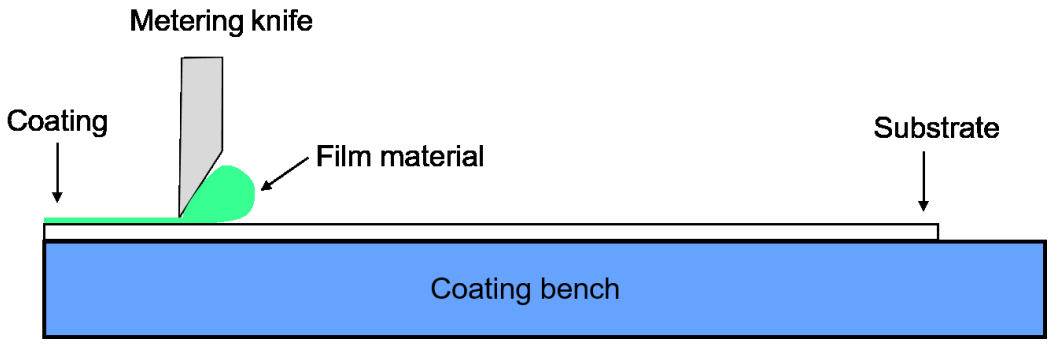

Figure 10: Schematic of the laboratory coating setup.

3.3 Characterization

3.3.1 Wet film thickness

The wet film thickness measurement was the most vital characterization in the entire study and was done using various methods, in order to compare the results. The indicative reference thickness values were estimated using comb-type wet film gauges procured from TQC Sheen as described in ISO 2808:2007. Measured values from the contact-method were then compared with the non-contact method measurements. Three different non-contact methods were used in the study, namely, NIR spectroscopy, IR thermography, and optical confocal displacement sensing. All three methodologies for the non-contact measurements are described below.

NIR Spectroscopy

The FTNIR spectrometer system was manufactured by iRed Infrarot GmbH, Austria and was installed at the pilot facilities of Berndorf Band GmbH in Berndorf, Austria. The measurements from this system were taken at the facilities of Berndorf Band GmbH. Coatings were prepared using the abovementioned drawdown method and the samples were then manually placed over a moving steel belt. The steel belt was moving at a constant speed of 0.15 m/min and that allowed 20 minutes of drying time. Measurements on wet films were taken by the first optical sensor and then the sample moved into the drying tunnel. When the dried samples exited the tunnel, dry-end thickness measurements were taken by the second optical sensor. The measurement sensor consisted of a light source and a detector. The reflected signal from the sample was transmitted via a fibre optic cable to a multiplexer and onwards to a processor, where the signal was used to generate an absorption spectrum. Figure 11 schematically illustrates the overall operation of the system.

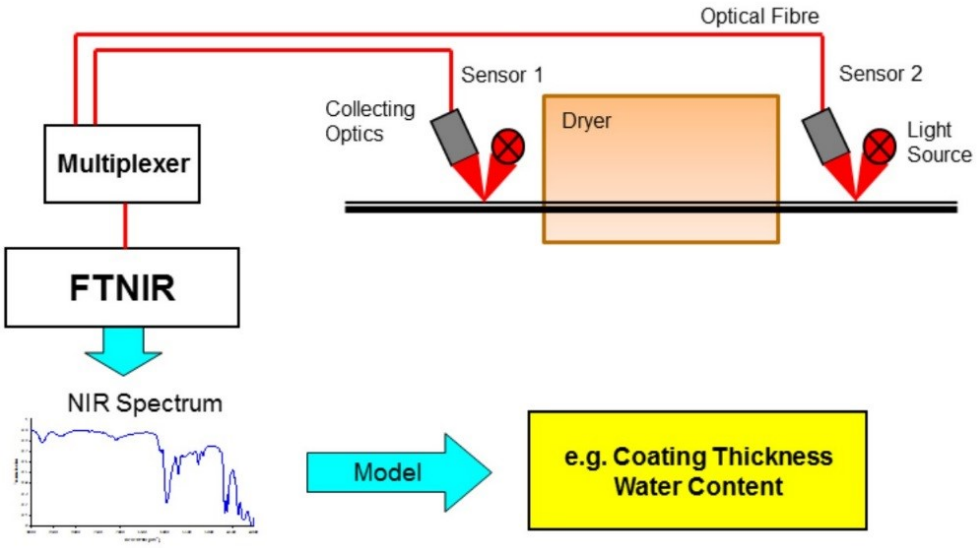

Figure 11: Schematic description of online operation of the FTNIR spectroscopic system.

It is important to note here that since the solids content of both the formulations was less than 2%, it was assumed that the wet film was composed totally of water. This assumption neglects the presence of other components of the film for thickness evaluation. Therefore, the spectrum peaks corresponding to water absorption wavenumbers, i.e. 5260, 6880 and 8330 cm^{-1} were identified, and the area under the peak was correlated to film thickness. The exact correlation algorithm is an intellectual property of the manufacturer and was not disclosed. The measurement parameters used in the study can be found in Table 3.

Table 3: Measurement parameters for FTNIR measurements

Measurement mode	Reflection
Spot diameter (mm)	25
Measurement distance (mm)	100
Measurement duration (s)	2
Wavenumber range (cm^{-1})	4000-10000
Resolution (cm^{-1})	3.7

IR Thermography

An infrared-responsive thermographic measurement system manufactured by Winterthur Instruments AG, Switzerland was used to determine the film thickness. The system worked in the active mode, implying that the sample was heated using external radiation and subsequently, the resultant IR radiation from the sample was measured. The measurement assembly consisted of a high-intensity halogen lamp that produced pulses of light energy in the range of 500-2000 J. The light energy from the source was directed to the sample using an annular opening that ensured homogenous sample heating in the measurement area. Photodetectors were positioned in the centre of the lens to enable vertical alignment with the heated area of the sample. Surface temperature of the sample was monitored continuously, and

the rate of cooling of the sample was correlated to the sample thickness. Figure 12 depicts the measurement assembly and principle schematically.

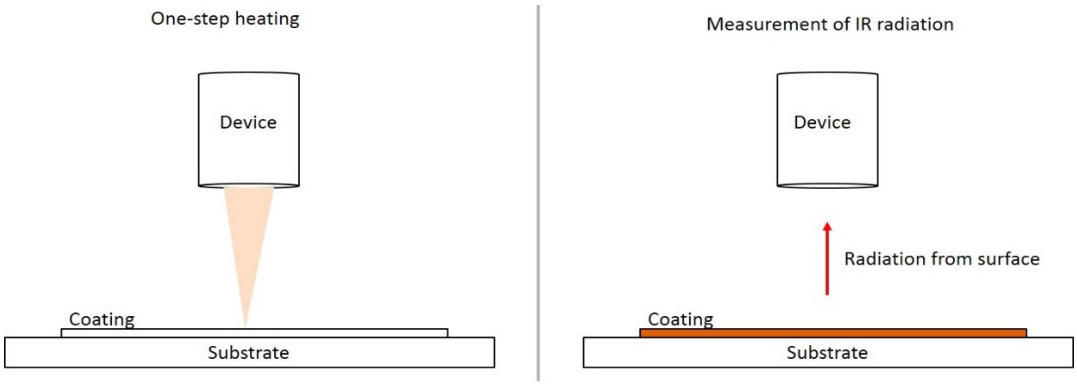

Figure 12: Schematic of the IR thermographic method.

All measurements using this system were performed inside a closed metal cage in order to prevent interference from external light sources and to protect the user from bright flashes during measurement. The measurement parameters used in the study can be found in Table 4.

While measuring MFC films, a very low SNR (30-40) was observed and hence, an optical reflection amplifier (ORA) was installed over the lens of the device. The ORA was a conical-shaped accessory which had a highly reflective inner surface which collected stray radiation and guided it to the IR detector. A higher signal intensity and SNR were observed after the installation of the ORA. Measurements were taken at five different spots on each sample for a duration of 60 seconds on each spot. Before using a new type of sample, the device was calibrated with two-point method, i.e. with two samples of known thickness.

Table 4: Measurement parameters for IR thermographic measurements

Measurement mode	Active pulsed
Spot diameter (mm)	22
Measurement distance (mm)	110
Measurement duration (ms)	20-200
Light energy (J)	1000-2000

Theoretically, thermographic measurements are not very sensitive to changing lift-off if the measurement SNR is maintained at a sufficient level. Nonetheless, for studying the effect of changing lift-off systematically, wet films drawn using 500 µm knife gap were used. The focal length of the lens used to converge incident radiation onto the sample was 135 mm, and the diameter of the lens was 120 mm. Hence, the spot size was derived to be only a function of the lift-off. The following equation relates the spot size to the lift-off:

$$s = \frac{d.(f - z)}{f}$$

where, s = measurement spot size, d = lens diameter, f = focal length of the converging lens, and z = lift-off from the sample surface.

Optical Confocal Displacement Sensing

An optical confocal measurement system was procured from Micro-Epsilon Messtechnik GmbH, Germany. The system consisted of two sensors connected to a signal processor via fiber optic cables. The processor was further connected to a computer via an Ethernet cable for control and data collection. All measurements were made in a two-sided geometry where the sensors were placed parallel and equidistant from the sample, on opposite sides. The system measured the distance of the sample from each sensor and calculated the thickness of the sample by subtracting the sum of the two distances from the total separation between the sensors.

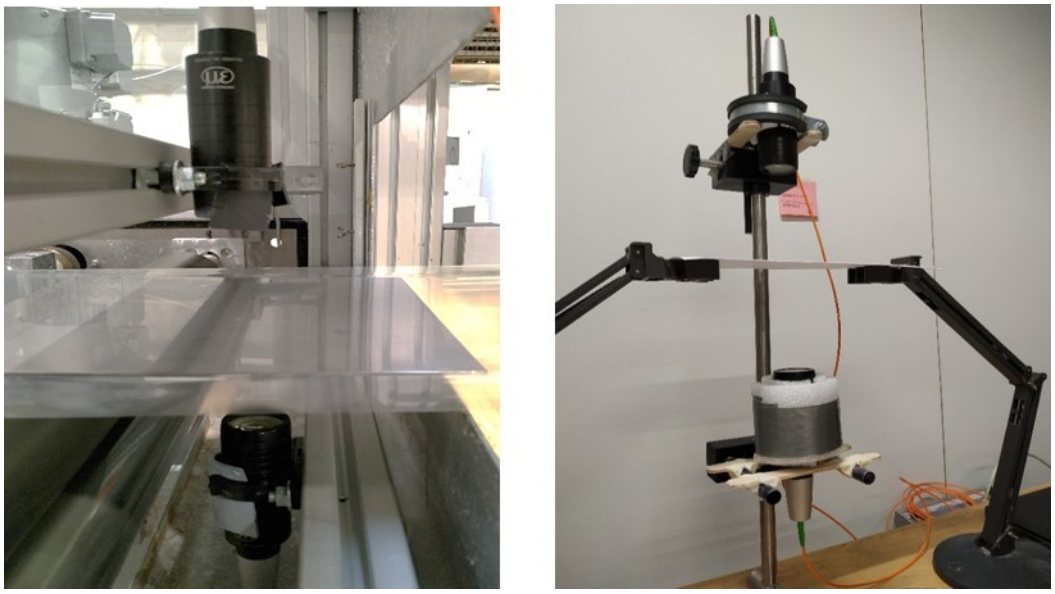

Figure 13: The experimental setups used for optical confocal measurements. For metal substrate (left) and for plastic and membrane (right).

Measurements were taken at five different spots on each sample for a duration of 60 seconds on each spot. An average value and standard deviation were calculated from the data and reported. The device was factory calibrated and did not require recalibration in case of changing film or substrate material.

Table 5: Measurement parameters for optical confocal measurements

Measurement mode	Reflection
Spot diameter (mm)	1-1.2
Measurement distance (mm)	65
Measurement duration (s)	60
Measurement rate (Hz)	1000

3.3.2 Dry film thickness

Dry film thickness (DFT) measurements were performed using three different methods. The reason behind using multiple methods was the varying adhesion of dry nanocellulose films to different substrates. Higher adhesion made separation of dry films from substrates more difficult, while in the case of lower adhesion, films were peeled easily from the substrates. Therefore, in cases where the dry film could be separated undamaged, the film thickness was measured using an L&W micrometer (TAPPI T 411). On the other hand, if the separation of film and substrate was not possible, the thickness of coated and uncoated parts of the substrate were measured and their difference was considered as the film thickness. For films on the metal substrate, it was not possible to use a micrometer to take readings from all over coated area due to large size of the samples. Therefore, an inductive thickness measurement gauge Elcometer 456 Top, supplied by Elcometer Instruments Ltd., U.K., was used to measure film thickness on the metallic substrate. Table 6 lists the characterization method used for each combination of film material and substrate used in the study. All samples were conditioned at 23°C and 50 % relative humidity for at least 24 hours before taking any thickness measurements, in order to minimize any effect of moisture on the final results. Thickness was measured at ten spatially different points for each sample for observing variations. All three non-contact methods described above were also used for measuring dry film thickness of the samples using the same procedure.

Table 6: Dry film thickness characterization methods

Film Material	Substrate	Dry film characterization method
CNF	Plastic	Micrometer
CNF	Membrane	Micrometer; on peeled film
CNF	Steel	Inductive
MFC	Plastic	Micrometer
MFC	Membrane	Micrometer; on peeled film
MFC	Steel	Inductive

3.3.3 Other characterization

All rheology measurements were performed on a stress-controlled rotational rheometer (Paar Physica MCR 301), manufactured by Anton Paar GmbH, Austria. Parallel plate geometry was used (50 mm plate diameter) at 1 mm plate gap to obtain data for both, shear flow and viscoelasticity curves. For all measurements, samples were pre-sheared at 100 s^{-1} for one minute and were then left idle for two minutes before starting the final measurements, a protocol suggested by Naderi et al. [98] and Kumar et al. [99]. This protocol ensures homogeneity in the sample. For shear flow measurements, shear rate range of 1-1000 s^{-1} was chosen for both nanocellulose recipes and ten seconds measurement time was allowed for each data point. For viscoelasticity curves, the linear viscoelastic (LVE) region was identified by conducting oscillatory strain sweep tests in the strain range of 0.01-100 % at a constant frequency of 10 Hz. Subsequently, frequency sweeps were performed in a frequency range of 0.1–100 Hz, while keeping the strain fixed at 0.5 %, i.e. within the LVE region. Measurement time was 10 seconds per point in both types of

viscoelastic measurements. All samples were brought to a constant temperature of 23°C before any measurements were made.

Black coloured backgrounds for IR thermographic measurements were prepared by printing RGB (0,0,0) on 100 gsm Mondi Colour Copy paper using a commercial Canon ImageRunner Advanced C5250i printer. To characterize the printed colour, colour measurements were made using a Datacolor ELREPHO spectrophotometer using a daylight (D65) type illuminant at 10° angle of incidence to the sample.

4. Results and Discussion

4.1 Rheology

Rheology of the film material plays a vital role in all coating processes and a sufficient understanding of flow behaviour is needed to ensure uniform defect-free coatings. In regard to nanocellulose suspensions, they have been shown to exhibit a high yield stress and a highly shear-thinning behaviour. Even at low consistencies, nanocellulose suspensions exhibit a high zero-shear viscosity. Rheology measurements were done on both coating formulations in order to determine the apparent viscosity of the suspensions during coating. Using a drawdown coater speed of 3 m/min, the shear rates at knife gaps of 700, 500 and 300 µm were approximately 71, 100 and 167 s^{-1}, respectively.

Figure 14 shows the highly shear thinning behaviour of both formulations and indicates the apparent viscosity of the suspensions in the applied shear rate range. It can be observed from the figure that the shear flow curve for CNF starts at a lower value than that of MFC and that happened since the CNF suspension was at a lower consistency (1.5% as compared to 2% for MFC). Additionally, a 'kink' observed in the MFC curve at ca. 10 s^{-1} is a prominent feature of MFC shear flow curves. Karppinen et al. [100] imaged the flow of MFC suspensions and showed that soft fibrillar flocs are present in the suspensions at low shear rates. As the shearing increases, the flocs grow in size and thus, offer a greater resistance to the flow, leading to the plateau in the flow curve. With further increase in shearing, the flocs are broken and fibrils get aligned with flow streamlines, causing a decrease in viscosity subsequent to the plateau region. The power law index for the MFC curve was 0.31, when calculated after the plateau region, i.e. 20 s^{-1}. The power law index for CNF was calculated to be 0.14, indicating higher shear-thinning in the CNF formulation as compared to the MFC formulation.

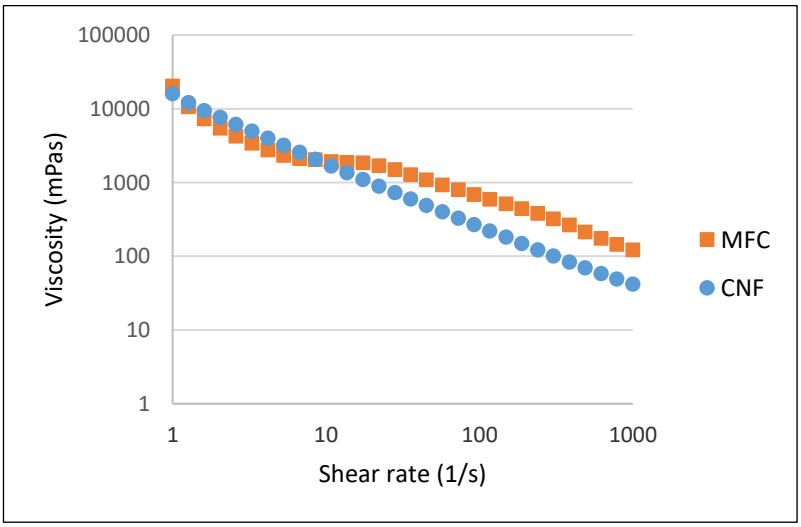

Figure 14: Shear flow behaviour of MFC and CNF formulations.

In addition to shear flow, viscoelastic behaviour of the formulations was also studied. Amplitude sweeps for both formulations are shown in Figure 15 which

helps in the determination of the LVE. Additionally, the gel-like structure of both formulations can be observed as the storage modulus (G′) is higher than the loss modulus (G″) in each case. From Figure 16, we can note that the CNF suspension has more pronounced gel-like structure as compared to the MFC suspension, as the phase angle is lower. This behaviour can be attributed to the nanosize fibrils present in the CNF suspension which swell more than microsize MFC fibrils.

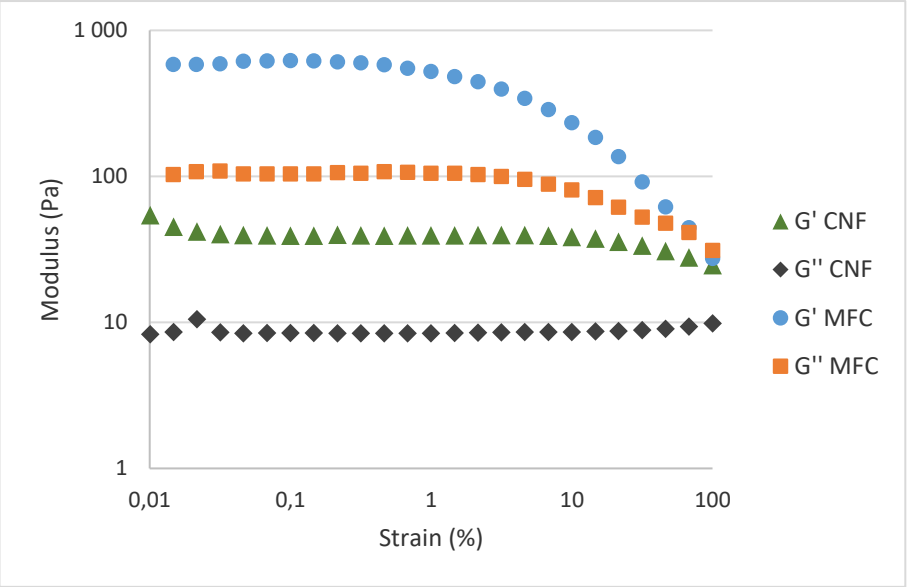

Figure 15: Amplitude sweep for CNF and MFC.

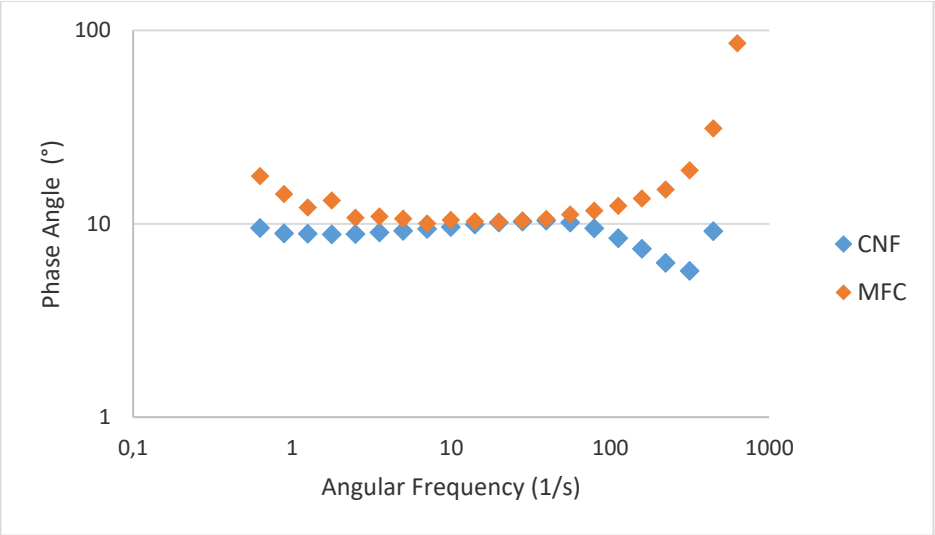

Figure 16: Frequency sweep for CNF and MFC.

4.2Offline measurements

Reference samples of dry films were prepared once and used for comparison of measurement data from the three non-contact techniques. On the contrary, wet film samples were prepared each time before measurements, since the studied measurement systems were not available to be used parallely. The dry film thickness (DFT) of samples measured with the contact methods is tabulated in Table 7, and these values have been treated as reference values for comparison with non-contact methods. It can be seen that DFT for CNF formulations on same substrate and same gap, is lower than that of MFC suspensions. This is explained by the lower consistency of the CNF suspension than that of the MFC suspension.

Table 7: DFT using contact methods

Film Material	Substrate	Knife gap used (µm)	Thickness (µm)
CNF	Steel	700	7.1 ± 1.4
	Steel	500	4.2 ± 1.2
	Steel	300	2.8 ± 0.9
	Membrane	700	11.4 ± 0.8
	Membrane	500	3.6 ± 1
	Membrane	300	2 ± 1.8
	Plastic	700	6.2 ± 1.3
	Plastic	500	4.6 ± 1.2
	Plastic	300	3.6 ± 0.5
MFC	Steel	700	14 ± 1.4
	Steel	500	11.6 ± 0.5
	Steel	300	8.4 ± 0.8
	Membrane	700	18.4 ± 1
	Membrane	500	15 ± 0.6
	Membrane	300	9.2 ± 2.8
	Plastic	700	17.8 ± 0.7
	Plastic	500	15.4 ± 0.5
	Plastic	300	7.6 ± 1

Wet film thickness (WFT) of all sample types determined from contact method (comb-type gauges) is listed in the table below. It can be seen from Table 8 that the WFT on membrane is the lowest among all substrates for both formulations. This is observed because membrane is the only porous substrate among the three and absorbs a portion of the film material.

Table 8: WFT using contact method

Film Material	Substrate	Knife gap used (µm)	Thickness (µm)
CNF	Steel	700	550
	Steel	500	380
	Steel	300	120
	Membrane	700	250
	Membrane	500	225
	Membrane	300	50
	Plastic	700	600
	Plastic	500	470
	Plastic	300	280
MFC	Steel	700	550
	Steel	500	450
	Steel	300	240
	Membrane	700	520
	Membrane	500	380
	Membrane	300	180
	Plastic	700	650
	Plastic	500	470
	Plastic	300	260

4.3 Non-contact measurements and data validation

Three techniques were used for non-contact thickness measurements. Performance of the techniques was evaluated by calculating the absolute and relative error in the measurement for each sample. The calculated values for errors can be found in the appendix. Additionally, the measurement data from each technique was used to calculate the root mean square (RMS) error for both wet and dry film measurements. In further discussions, the measurements taken using contact and non-contact methods are denoted by adding letters ‘C’ and ‘NC’ to the sample names. If the text is being read from a black and white or a greyscale print, the graphs in the further text can be read by following the histogram for each knife gap from left to right. The legend is marked in the same order for each figure.

NIR Spectroscopy

For NIR spectroscopic measurements, a different set of knife gaps was used, i.e. 700, 300, and 100 µm, as compared to the other two techniques. The third data point was chosen to be 100 µm for these measurements in order to test the accuracy of the system to measure thin films. Figure 17 shows the comparison between the thicknesses obtained from contact and non-contact methods. Non-contact thickness data for film formed at 100 µm gap on plastic is not available because the system was not able to measure the thickness of these films. Nonetheless, a more informative observation is that the measurement error is the highest for films casted on the membrane. Since the membrane absorbs water and the device measures thickness based on water content, the device fails to identify the location of the substrate. This implies that a difference in IR absorption spectra must be observed at the physical boundary between the film and the substrate in order to accurately determine film thickness.

Based on this inference, it can be expected that erroneous measurements would be observed on all substrates that absorb the film material if corrections for the amount of absorbed film material are not made. For instance, measurements made on nanocellulose coatings on paperboard are expected to be inaccurate. Since the thickness calculation model of the system is based on measuring water content in the film, it was expected that the model would not be accurate at low water contents, i.e. for dry films. Figure 18 confirms this as we can observe that the measured thickness values using non-contact method are much higher than the actual values. Additionally, the instrument did not generate any thickness response for dry films on steel and plastic and the response generated on membrane could possibly be an error. This information suggests that an evaluation model based on the concentration of some other species, such as cellulose, could be more accurate for DFT measurements.

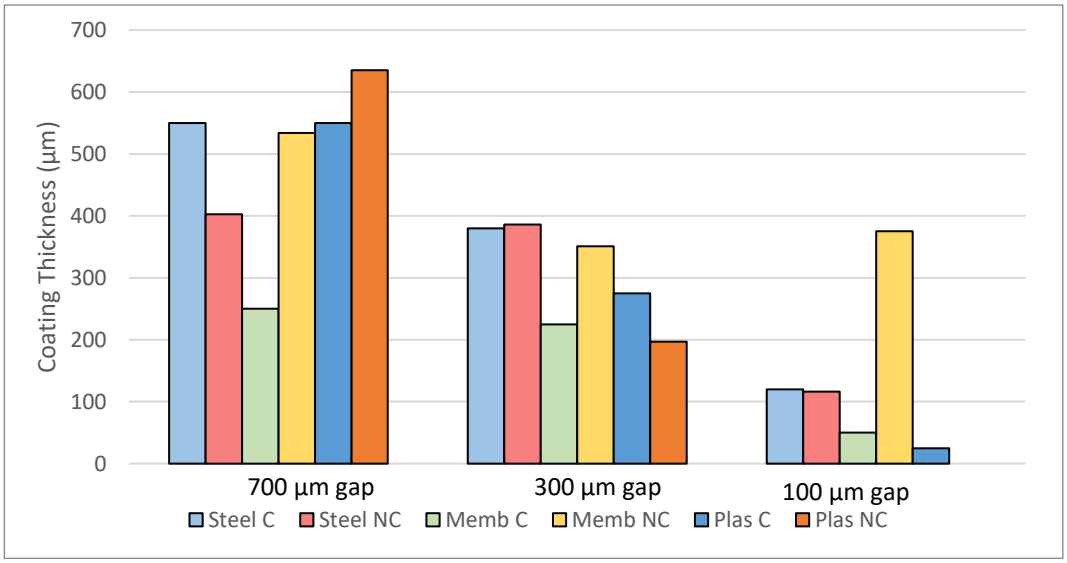

Figure 17: WFT measurements for CNF using NIR spectroscopy.

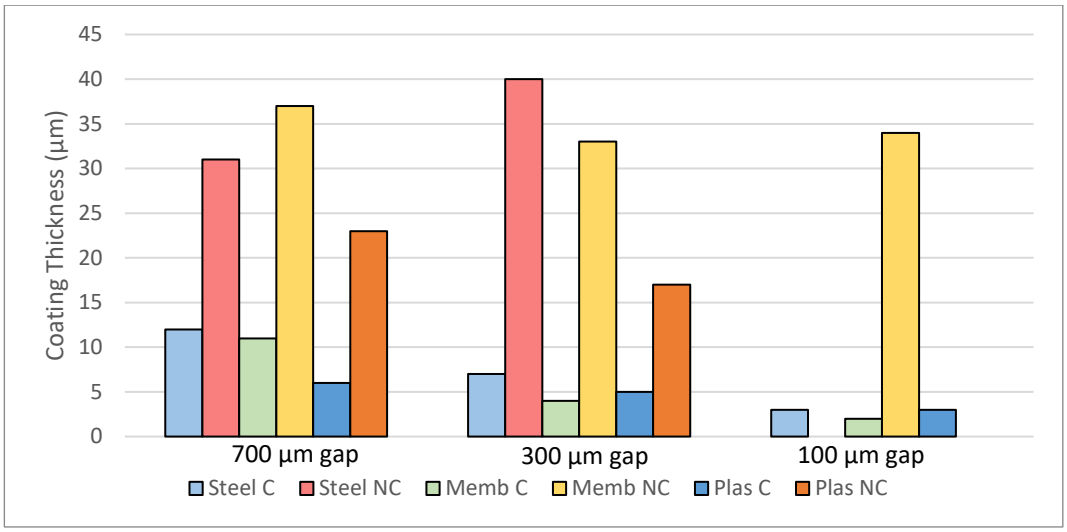

Figure 18: DFT measurements for CNF using NIR spectroscopy.

A similar trend was observed while using MFC as the film material. The non-contact technique showed higher thickness than the actual value for all cases except for films made at 300 µm gap on plastic substrate (Figure 19). However, Figure 20 shows that for dry MFC films, the trend is similar to the one observed for dry CNF films, with no exception. It can be noted that films prepared using all the knife gaps could be measured in the case of MFC. This might have been possible due to a thicker film deposition due a relatively higher viscosity and solids content of the MFC formulation as compared to the CNF formulation.

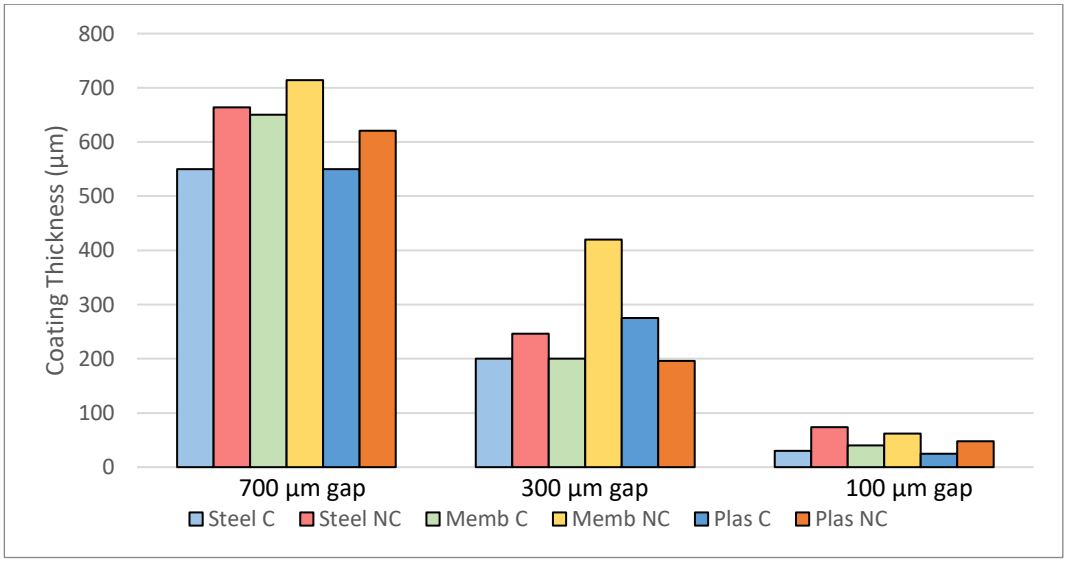

Figure 19: WFT measurements for MFC using NIR spectroscopy.

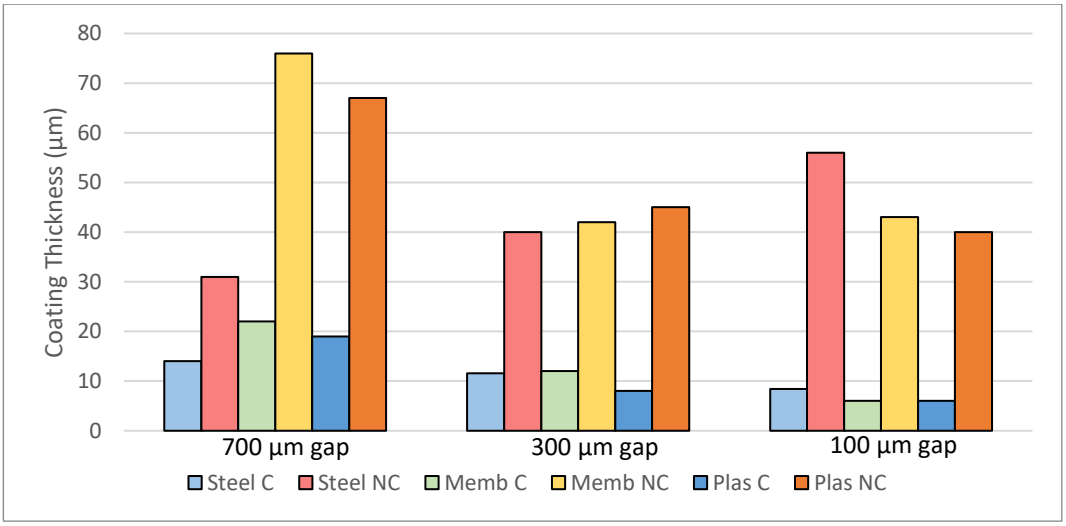

Figure 20: DFT measurements for MFC using NIR spectroscopy.

Based on the above data, it can be concluded that the measurement technique is independent of the colour of the film material. Chemically similar substances are measured in a similar manner and that could be beneficial in certain cases, such as formulations containing a variety of nanocelluloses. However, the results are highly dependent on the evaluation model. The general accuracy of the technique was poor and the RMS error for wet CNF films was 164 µm and for dry films, the value was 25 µm. For MFC, the RMS error values were 95 and 38 µm for wet and dry films, respectively. These errors are large and make the NIR spectroscopy method, used in the manner as described in the current work, unsuitable for precise quality control. However, improvements in the evaluation model might reduce the errors and the technique can be made suitable for precise measurements on rigid, non-absorbing substrates.

IR Thermography

IR thermography was the second technique to be studied. The measurement system was studied using samples prepared using knife gaps of 700, 500, and 300 µm. The performance of the thermographic system was found to be better as compared to the spectroscopic system. Figure 21 shows that the measurements were quite accurate for wet CNF films on steel at 500 and 300 µm gaps. A reasonable accuracy can also be observed for films on plastic at 700 and 500 µm gaps and on membrane at 300 µm gap. The results do not appear to follow any general trend.

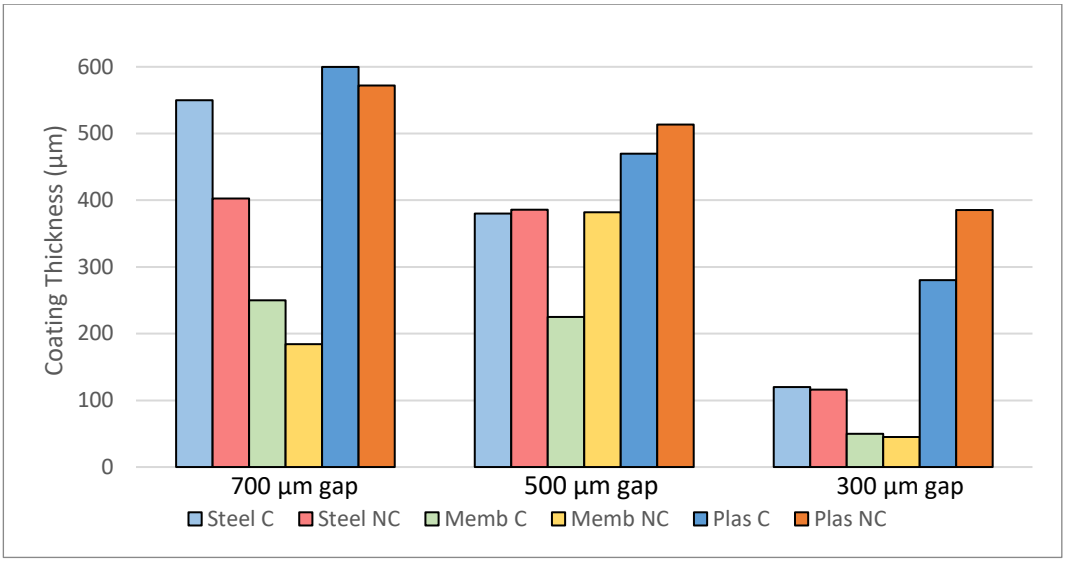

Figure 21: WFT measurements for CNF using IR thermography

Figure 22 shows the results for dry films where the proportional decrease in the thickness of films upon drying is observed. However, the magnitude of error for films on membrane is particularly noteworthy. The non-contact method gauges the thickness on membrane to be much higher than the actual value. This error might have occurred due to two reasons. Firstly, the dry adhesion between CNF and membrane was not good and the films got detached from the membrane surface upon drying. During measurements, care was taken to test only the samples in which the film stayed attached to the substrate but air might have entered between the film and membrane. In the presence of air, heat transfer dynamics in the system is disturbed and the cooling curve in the output signal starts to differ from the calibration curve. Secondly, the membrane is white in colour and the system registers a low SNR for white targets, possibly leading to incoherent results.

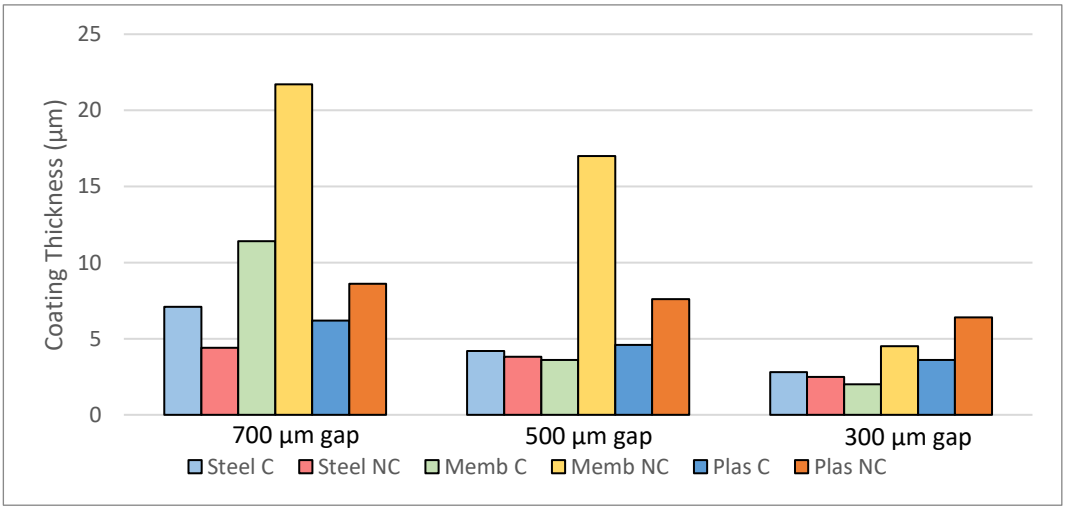

Figure 22: DFT measurements for CNF using IR thermography

From Figure 23, it can be observed that the measurement accuracy decreases with decreasing film thickness in case of films on plastic and the opposite happens in case of steel. Since steel has a high thermal diffusivity, it absorbs and radiates heat at a faster rate than water. The presence of essentially a water film over the steel surface retards the rate of cooling, hence lowering the intensity of the collected IR radiation. Thus, as the amount of film material on the steel surface reduces, the better the accuracy of measurement becomes. On the other hand, plastics respond slower to thermal effects than water and hence, the decreasing amount of water retards the thermal response further to result in a poor measurement accuracy.

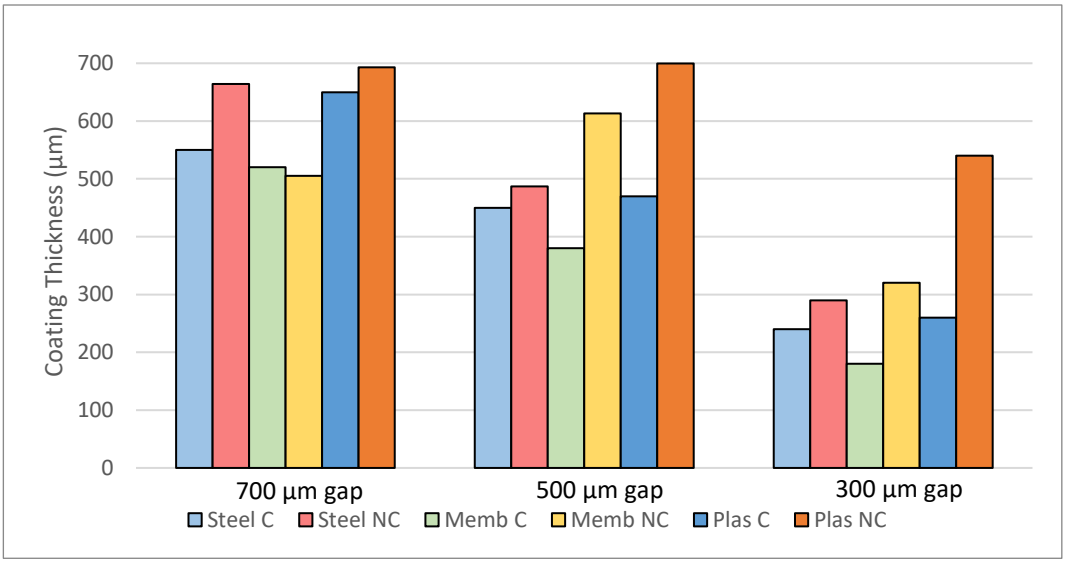

Figure 23: WFT measurements for MFC using IR thermography

Figure 24 shows large errors as the SNR in these measurements was very low even after the installation of ORA. The reason behind this is the same as described for Figure 22.

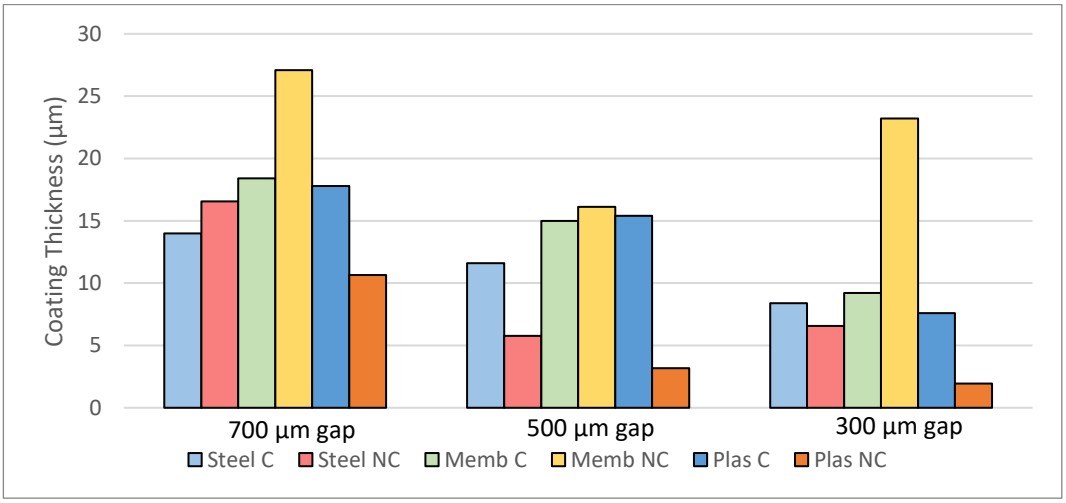

Figure 24: DFT measurements for MFC using IR thermography

The ORA was used primarily to study MFC films since the SNR was much lower than in case of CNF films in general. However, in certain cases the ORA was used for CNF films as well. To study the efficacy of the ORA, films were prepared using a knife gap of 500 µm on all three substrates and the SNR values were recorded with and without ORA. It can be observed from Figure 25 and Figure 26 that SNR increases for each combination of film and substrate, both in wet and dry state. An interesting result from this experiment was that the average increase in SNR was more for dry films as compared to wet films. This implies that a larger portion of radiation from the samples was being left undetected in case of dry films. Since the ORA just acts as a radiation collector, samples which allow a smaller portion of incident energy to travel radially in the sample, should allow a higher increase in SNR. Cellulose has an extremely low thermal conductivity (0.0035 W/m.K at 10°C) as compared to water (0.578 W/m.K at 10°C) and thus, dry films which can be assumed to consist totally of cellulose, conduct less heat in the radial direction. Thus, a higher elevation in SNR is observed in dry films as compared to the wet ones, which are mainly composed of water.

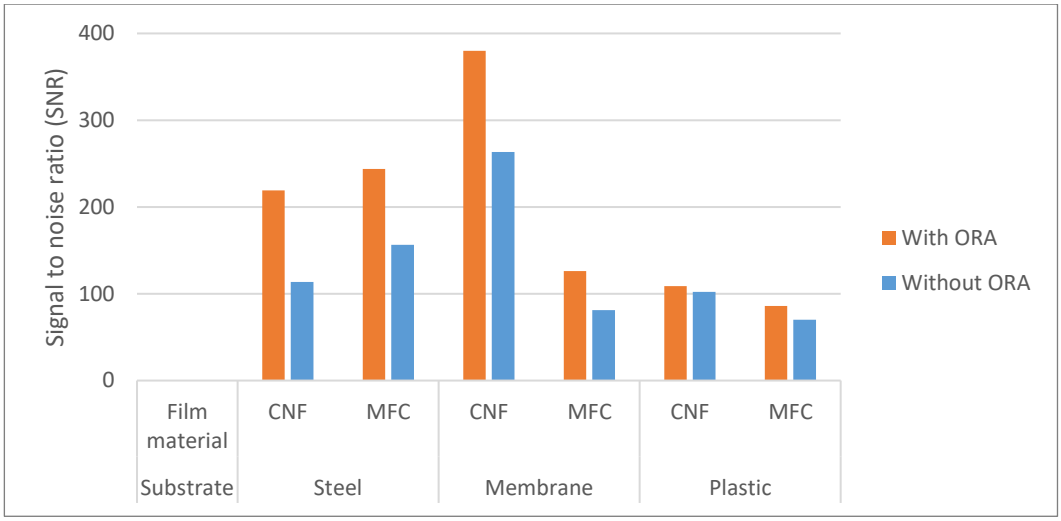

Figure 25: Effect of ORA on SNR for wet films

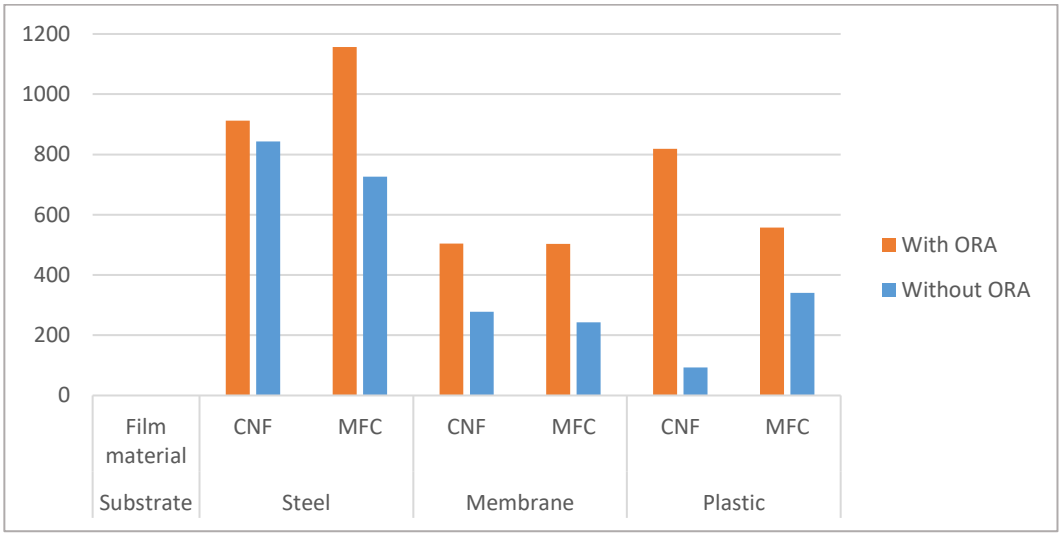

Figure 26: Effect of ORA on SNR for dry films

The performance of the device was sensitive to both optical and thermal properties of the target. During calibration, the thermal properties are measured and stored by the device, but the effect of optical properties is not taken into account as it is considered negligible. Hence, the effect of changing background colour was studied, but it was possible only with a transparent substrate, i.e. plastic in the current study. A black background (BBG) and a white background (WBG) were used in the study where the positions of the colours on the CIELAB space were (21.13, -0.01, -0.79) and (94.71, 3.45, -14.67), respectively. Figure 27 shows that using a BBG allows a SNR value an order of magnitude greater than that in case of using WBG. Also, dry films allow a higher SNR due to lower reflection from the sample in absence of water in the films.

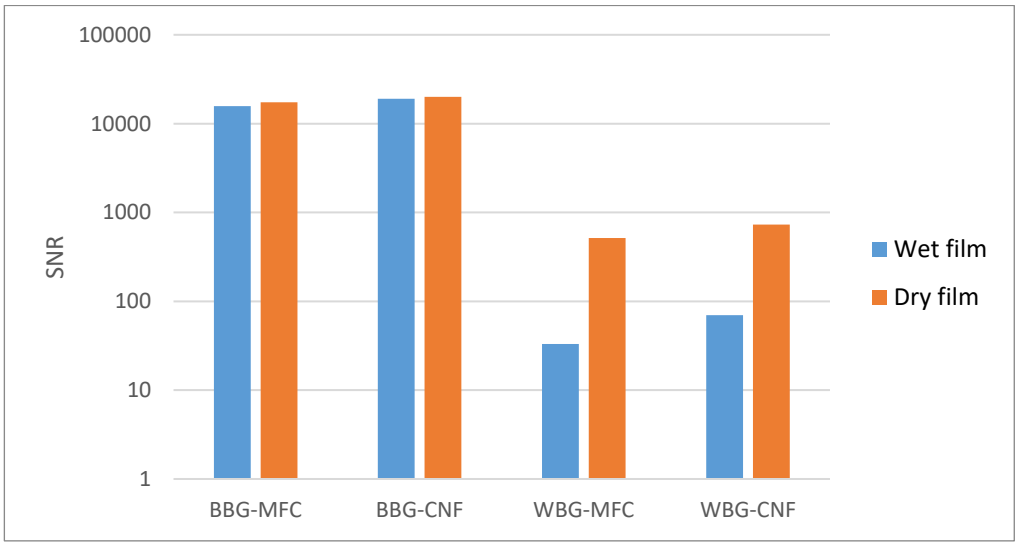

Figure 27: Effect of changing background colour on SNR

For studying the effect of changing lift-off on measurement SNR, the lift-off range of 80-180 mm was used. Figure 28 illustrates that spot size follows a linear relationship with lift-off, and the curve is symmetric around the focal point, i.e. 135 mm. Additionally, the figures also show that for all substrates, SNR gradually decreases with increasing distance between the sample and the detector. This result was expected since intensity of electromagnetic radiation follows an inverse square relationship with distance, and the detector receives a lower signal amplitude. An interesting observation is that for membrane and plastic substrates, CNF exhibits a higher SNR than MFC but for steel, the opposite holds true. A reason behind this might be that since the wet films were glossy and the lift-off was much lower than the focal length, the effect of colour of film material was dominated by reflection from the film surface.

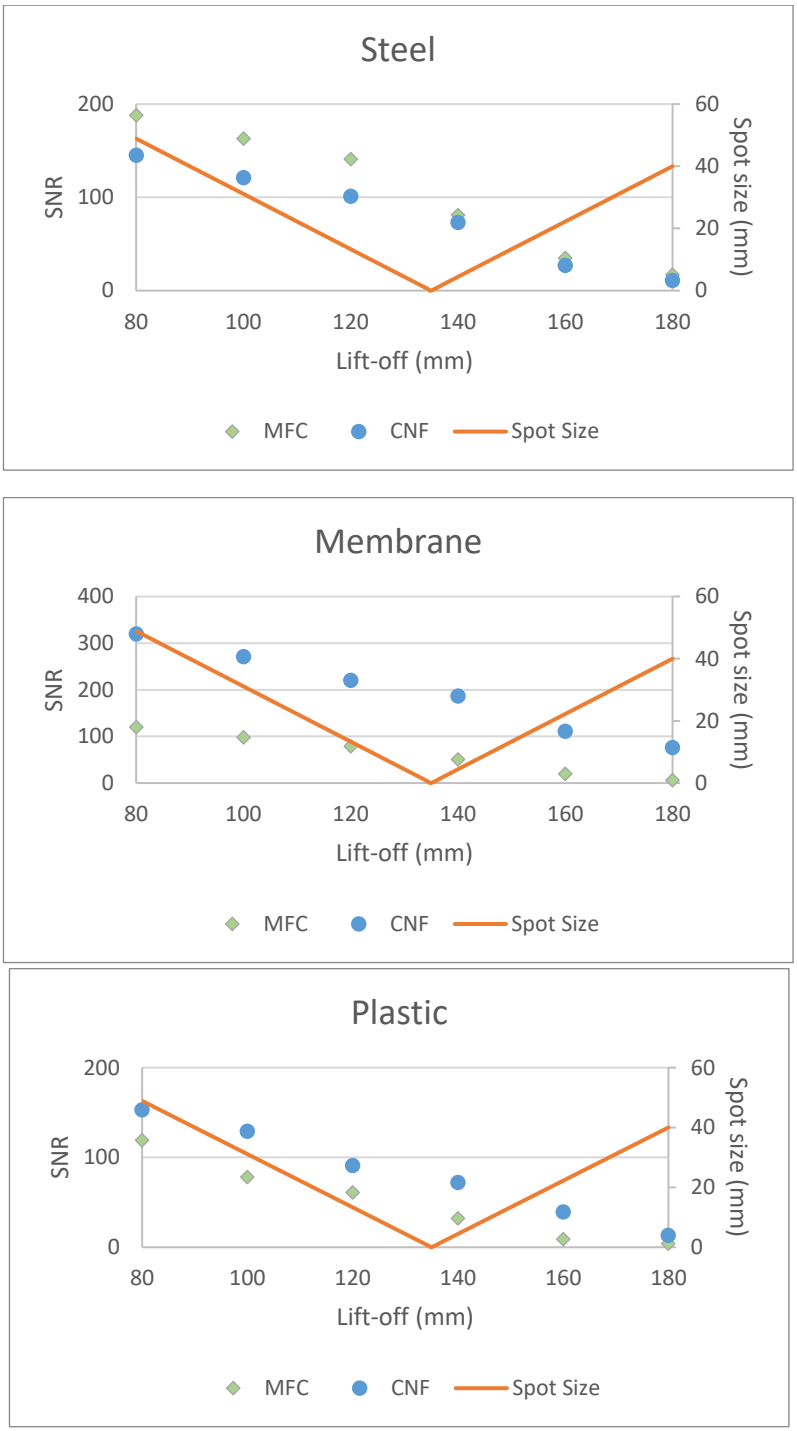

Figure 28: Effect of changing lift-off on SNR and measurement spot size.

Optical Confocal Displacement Sensing

The third and last technique to be tested was optical confocal displacement sensing. As the earlier two methods were based on mathematical evaluation of the output signals to calculate thickness, the third method was chosen to be more direct, i.e. primarily measuring distances. Optical confocal method is a relatively new technique in the market dominated by laser-based methods. Laser-based methods are unable to measure small displacements using low-intensity lasers (typically less than 5 mW) and the use of high-intensity lasers is not recommended in order to protect the product from damage. Optical confocal devices use low-intensity white light and can detect displacements even in the sub-micron range. Therefore, the optical confocal method was chosen.

The confocal method also faced the obstacle typically associated with purely optical methods, i.e. inability to measure transparent targets. This is evident from Figure 29 where the non-contact method failed to identify the position of the top surface of the liquid film. The reflected signal is then either obtained directly from the surface of the substrate or from a 'pseudo-surface' that the device incorrectly detects. For instance, in case of CNF films on plastic substrate, the device detects a pseudo-surface above the film-substrate interface. Such errors occur due to refraction of light upon entering the transparent film material. The non-contact measurement values in Figure 30 may also be considered erroneous due to the same reason. However, the device has not been designed to measure transparent targets and such performance was expected.

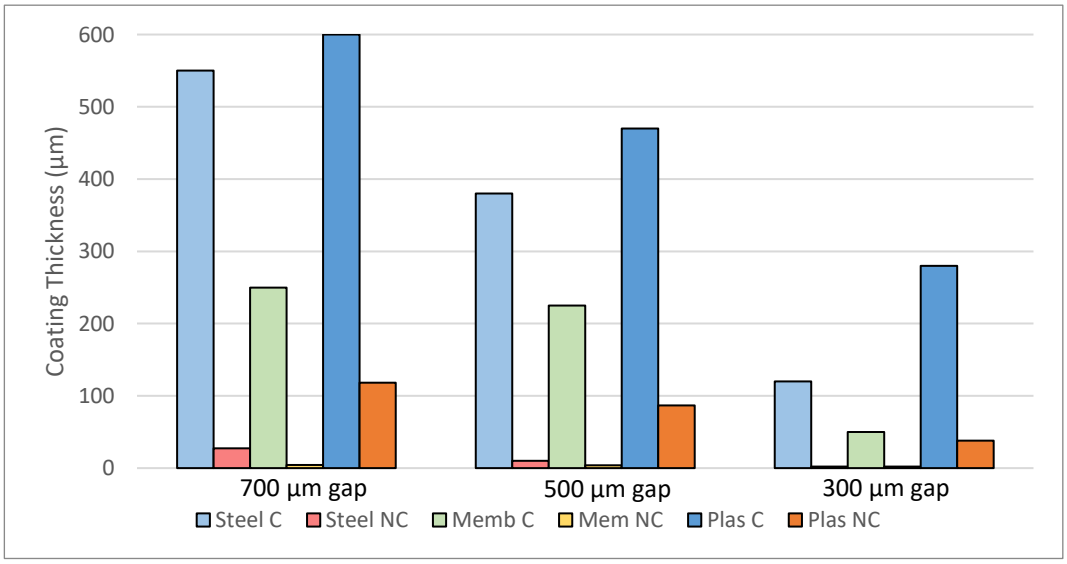

Figure 29: WFT measurements for CNF using optical confocal system

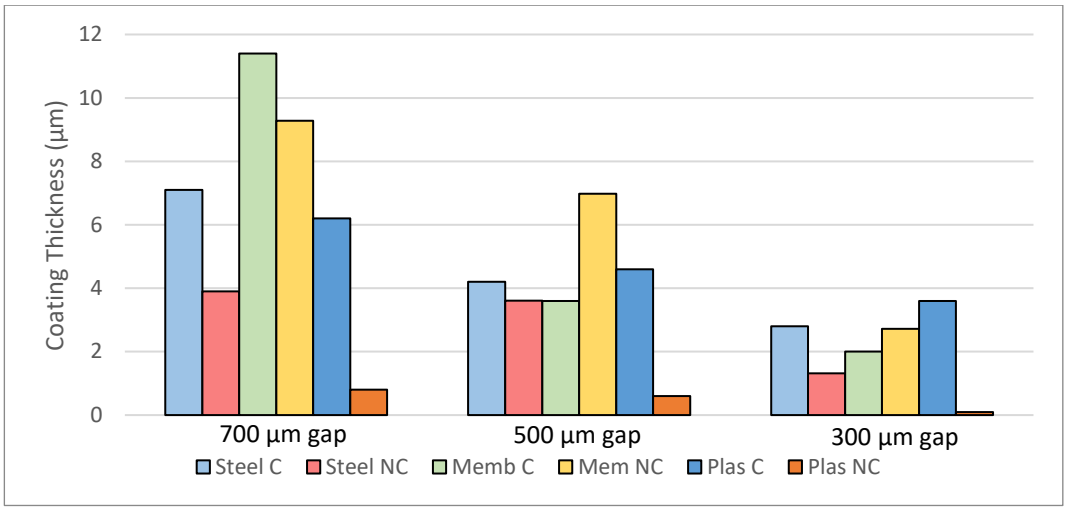

Figure 30: DFT measurements for CNF using optical confocal system

The actual performance assessment of the confocal system was done using MFC. The film material in this case was not transparent and can be considered as optically opaque. This property can be explained by high backscattering of incident light caused by fibrils. Thus, the device is able to determine the position of the top surface of the film relative to the bottom side of the substrate. Therefore, calibrating the system against the thickness of the substrate allowed the determination of film thickness. Figure 31 confirms the expected performance from the system, and the best performance among all methods was obtained from the system. The device was able to measure wet films with a good accuracy on all substrates and at all knife gaps. Figure 32 shows that the confocal system is able to accurately measure even small thicknesses. Marginal errors observed in case of dry films are due to translucent nature of MFC films, however, the magnitude of errors is within an acceptable margin.

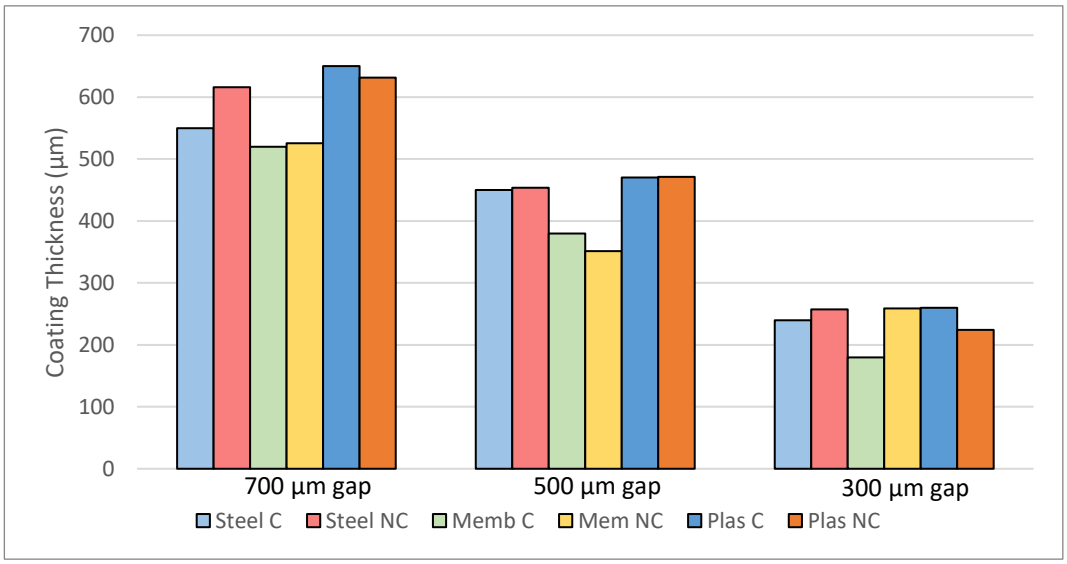

Figure 31: WFT measurements for MFC using optical confocal system

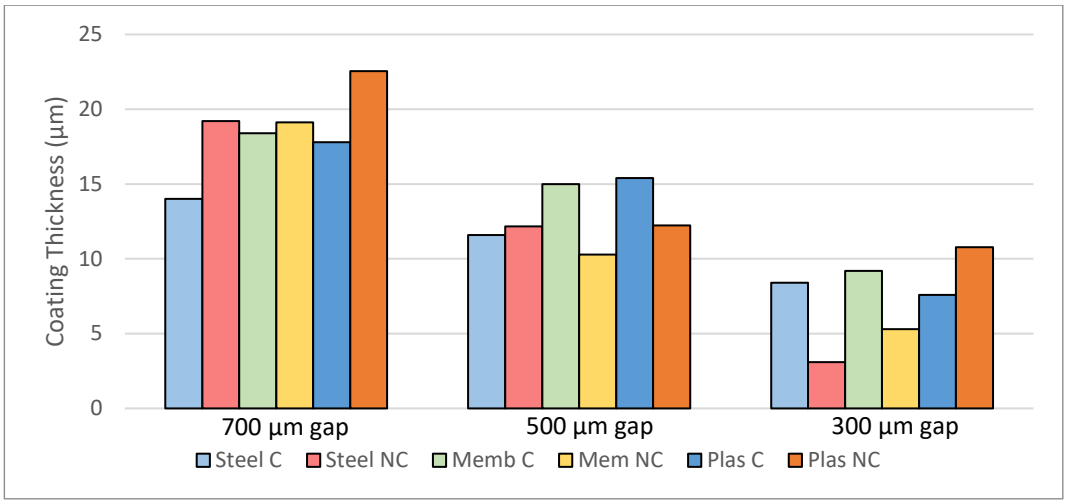

Figure 32: DFT measurements for MFC using optical confocal system

Comparison of techniques

Comparison of the three techniques can be made quantitatively by comparing the accuracy while measuring the thickness of nanocellulose films and coatings. Table 9 lists the RMS errors for all wet films, wet films of CNF, and wet films of MFC. Comparison of errors individually for CNF and MFC allows making decisions specifically for the materials and the overall error allows assessment of the technique for wet nanocellulose coatings in general. The same idea is also followed in Table 10. It is notable that the optical confocal method produced the most accurate measurements among the three techniques for MFC, both in dry and wet state. Whereas, for wet CNF films, IR thermography was the most accurate technique. For dry CNF films, both thermography and confocal methods appear to produce low errors but the performance of the confocal method remains dubious due to the pseudo surface effect explained in the above section.

Table 9: RMS errors for wet film measurements (all values in micrometers)

Material / **Technique**	All wet films	CNF	MFC
NIR Spectroscopy	130.06	164.23	95.36
IR Thermography	126.65	84.71	157.81
Optical Confocal Displacement Sensing	234.13	328.86	38.55

Table 10: RMS errors for dry film measurements (all values in micrometers)

Material / Technique	All dry films	CNF	MFC
NIR Spectroscopy	33.34	24.80	38.55
IR Thermography	6.95	5.98	7.81
Optical Confocal Displacement Sensing	3.51	3.10	3.89

5. Conclusions

In this work, non-contact measurements of coating thickness for nanocellulose-based films and coatings were performed. Two different types of nanocellulosic materials, namely, microfibrillated cellulose (MFC) and cellulose nanofibrils (CNF) were used. Three non-contact methods, viz. NIR spectroscopy, IR thermography, and optical confocal displacement sensing were used to measure thickness of nanocellulose coatings, both in dry and wet state. The results were then compared with those from contact measurements to calculate the accuracy and error. Moreover, the measurement results were analysed closely and reasons behind certain behaviour of instruments were explored.

NIR spectroscopy proved to be unsuitable for measuring thickness of nanocellulose films. The performance of the technique was highly dependent on mathematical models and assumptions used for deriving the thickness value from the measured parameter. Since the technique was based on measurement of amount of water in the film, any fluctuations in the homogeneity of the film formation reflected directly in the coating thickness value. Additionally, formulations with poor water retention might pose a challenge to proper measurements as the instrument would measure the thickness of only the separated water layer. FTNIR hardware technology is quite mature, but room for development exists on the software side. The measurement optics were compact in size and could be integrated easily in an online process. A single data processor could be utilized to analyse signals from multiple sensors through fiber optic cables, lowering the overall cost of the measurement system. Furthermore, measurements were not affected by vibrations of the production line or fluttering of the target substrate.

The biggest advantage of using NIR spectroscopy is that it offers more than one utility. The device can be used to analyse the chemical composition of both the coating and the substrate. For instance, homogeneity of the film material can be assessed in-process. It can also be used to monitor the moisture content of the film. Finally, the same device can analyse thickness of the films. Although the thickness measurements were observed not to be accurate in the current work, developments in the future regarding improved calculation models can help this technique become a multi-purpose offering for industrial coatings.

IR thermography is a novel and interesting technique, but it did not perform satisfactorily. Measurements were highly sensitive to colour of the target materials and the device calibration using two-point method took a long time. The device was bulky and its installation on industrial machines could be a challenge. In addition, a light shade needs to be installed along with the device due to a periodic emission of bright flashes of light during measurements. The measurement rate was low with only one measurement possible every four seconds when using the highest possible excitation energy, i.e. 2000 J. The device proved to work poorly for MFC films and produced the best results when used to measure CNF films on steel substrate. The performance for CNF films on membrane was also good.

Optical confocal displacement sensors are designed exclusively to measure miniscule displacements of opaque objects. The technique directly measures the dimensions of the target independent of any evaluation models. The utilization of optical confocal displacement sensors as a thickness measurement device proved to be highly successful for MFC films but it performed extremely poorly for CNF films. Accurate results were obtained while measuring wet MFC films on steel and plastic. The system was fairly simple to use and just involved plug-and-play. The measurement optics were compact and could be installed even in tight spaces in the process. This system is less expensive in comparison to the other two techniques. On the other hand, the drawbacks of the technique include its inability to measure transparent targets, its high sensitivity to vibrations on the machine or the web, and its small measurement range (0-3 mm).

The optical confocal technique worked with the best accuracy in the current work, but that does not limit the utilization of other techniques for nanocellulose film thickness measurements. Suitability of a technique for in-process measurements depends on a variety of factors, such as cost, desired accuracy, space restrictions, process speed, ambient conditions in the process, operational simplicity, etc. and there cannot be a single device which can fulfil all the requirements. Therefore, a combination of multiple techniques could potentially be used to create a robust online control system equipped with feedback loops. Multiple devices could be used to validate or correct the performance of each other or to be used specifically in certain process conditions. As more and more applications of nanocellulose are being developed and the market gears up for accepting nanocellulose-based products in daily life, it is expected that the need for process control systems for nanocellulosic materials will arise in the near future. The introduction of nanocellulose-based films and coatings in industrial processes is imminent, and the current work aims to accelerate the adoption of nanocellulose in such applications.

6. References

[1] C. N. Cutter, “Opportunities for bio-based packaging technologies to improve the quality and safety of fresh and further processed muscle foods,” *Meat Sci.*, vol. 74, no. 1, pp. 131–142, 2006 .

[2] C. J. Weber, V. Haugaard, R. Festersen, and G. Bertelsen, “Production and applications of biobased packaging materials for the food industry,” *Food Addit. Contam.*, vol. 19, no. SUPPL., pp. 172–177, 2002 .

[3] X. Z. Tang, P. Kumar, S. Alavi, and K. P. Sandeep, “Recent Advances in Biopolymers and Biopolymer-Based Nanocomposites for Food Packaging Materials,” *Critical Reviews in Food Science and Nutrition*, vol. 52, no. 5. Taylor & Francis Group, pp. 426–442, May-2012.

[4] J.-W. Rhim, “Critical Reviews in Food Science and Nutrition Natural Biopolymer-Based Nanocomposite Films for Packaging,” *Food Sci. Nutr.*, vol. 47, no. 4, pp. 411–433, 2007 .

[5] K. Petersen *et al.*, “Potential of biobased materials for food packaging,” *Trends in Food Science and Technology*, vol. 10, no. 2. Elsevier, pp. 52–68, 01-Feb-1999.

[6] B. Andres, S. Forsberg, C. Dahlström, N. Blomquist, and H. Olin, “Enhanced electrical and mechanical properties of nanographite electrodes for supercapacitors by addition of nanofibrillated cellulose,” *Phys. Status Solidi Basic Res.*, vol. 251, no. 12, pp. 2581–2586, 2014 .

[7] Q. Meng and I. Manas-Zloczower, “Carbon nanotubes enhanced cellulose nanocrystals films with tailorable electrical conductivity,” *Compos. Sci. Technol.*, vol. 120, pp. 1–8, 2015 .

[8] L. Valentini, M. Cardinali, E. Fortunati, L. Torre, and J. M. Kenny, “A novel method to prepare conductive nanocrystalline cellulose/graphene oxide composite films,” *Mater. Lett.*, vol. 105, pp. 4–7, 2013 .

[9] Plackett, “A review of nanocellulose as a novel vehicle for drug delivery,” *Nord. Pulp Pap. Res. J.*, vol. 29, no. 01, pp. 105–118, 2014 .

[10] J. K. Jackson, K. Letchford, B. Z. Wasserman, L. Ye, W. Y. Hamad, and H. M. Burt, “The use of nanocrystalline cellulose for the binding and controlled release of drugs.,” *Int. J. Nanomedicine*, vol. 6, pp. 321–330, 2011 .

[11] H. Martínez Ávila *et al.*, “Biocompatibility evaluation of densified bacterial nanocellulose hydrogel as an implant material for auricular cartilage regeneration,” *Appl. Microbiol. Biotechnol.*, vol. 98, no. 17, pp. 7423–7435, 2014 .

[12] S. Saska *et al.*, “Bacterial cellulose-collagen nanocomposite for bone tissue engineering,” *J. Mater. Chem.*, vol. 22, no. 41, pp. 22102–22112, 2012 .

[13] K. Kowalska-Ludwicka *et al.*, “Special paper – New methods
Modified

bacterial cellulose tubes for regeneration of damaged peripheral nerves," *Arch. Med. Sci.*, vol. 9, no. 3, pp. 527–534, 2013 .

[14] Z. Karim, M. Hakalahti, T. Tammelin, and A. P. Mathew, "In situ TEMPO surface functionalization of nanocellulose membranes for enhanced adsorption of metal ions from aqueous medium," *RSC Adv.*, vol. 7, no. 9, pp. 5232–5241, 2017 .

[15] H. Voisin, L. Bergström, P. Liu, and A. P. Mathew, "Nanocellulose-Based Materials for Water Purification," *Nanomaterials*, vol. 7, no. 3. Mar-2017.

[16] A. W. Carpenter, C.-F. de Lannoy, and M. R. Wiesner, "Cellulose Nanomaterials in Water Treatment Technologies," *Environ. Sci. Technol.*, vol. 49, no. 9, pp. 5277–5287, 2015 .

[17] S. H. Osong, S. Norgren, and P. Engstrand, "Processing of wood-based microfibrillated cellulose and nanofibrillated cellulose, and applications relating to papermaking: a review," *Cellulose*, vol. 23, no. 1, pp. 93–123, 2016 .

[18] A.- Isogai, T.- Saito, and H.- Fukuzumi, "- TEMPO-oxidized cellulose nanofibers," - *Nanoscale*, no. 1. p. 71.

[19] L. Wågberg, G. Decher, M. Norgren, T. Lindström, M. Ankerfors, and K. Axnäs, "The build-up of polyelectrolyte multilayers of microfibrillated cellulose and cationic polyelectrolytes," *Langmuir*, vol. 24, no. 3, pp. 784–795, 2008 .

[20] J. A. Sirviö, A. Kolehmainen, M. Visanko, H. Liimatainen, J. Niinimäki, and O. E. O. Hormi, "Strong, Self-Standing Oxygen Barrier Films from Nanocelluloses Modified with Regioselective Oxidative Treatments," *ACS Appl. Mater. Interfaces*, vol. 6, no. 16, pp. 14384–14390, 2014 .

[21] H. Liimatainen, M. Visanko, J. Sirviö, O. Hormi, and J. Niinimäki, "Sulfonated cellulose nanofibrils obtained from wood pulp through regioselective oxidative bisulfite pre-treatment," *Cellulose*, vol. 20, no. 2, pp. 741–749, 2013 .

[22] A. Pei, N. Butchosa, L. A. Berglund, and Q. Zhou, "Surface quaternized cellulose nanofibrils with high water absorbency and adsorption capacity for anionic dyes," *Soft Matter*, vol. 9, no. 6, p. 2047, 2013 .

[23] M. Pääkkö *et al.*, "Enzymatic Hydrolysis Combined with Mechanical Shearing and High-Pressure Homogenization for Nanoscale Cellulose Fibrils and Strong Gels," *Biomacromolecules*, vol. 8, no. 6, pp. 1934–1941, 2007 .

[24] M. Ankerfors, "Microfibrillated cellulose: Energy-efficient preparation techniques and key properties," KTH Royal Institute of Technology, 2012.

[25] N. Lavoine, I. Desloges, A. Dufresne, and J. Bras, "Microfibrillated cellulose - Its barrier properties and applications in cellulosic materials: A review," *Carbohydrate Polymers*, vol. 90, no. 2. Elsevier, pp. 735–764, 01-Oct-2012.

[26] A. F. F. Turbak, F. W. W. Snyder, and K. R. R. Sandberg, "Microfibrillated cellulose, a new cellulose product: Properties, uses, and commercial

potential," *J. Appl. Polym. Sci. Appl. Polym. Symp.*, vol. 37, pp. 815–827, 1983 .

[27] Y. Huang, C. Zhu, J. Yang, Y. Nie, C. Chen, and D. Sun, "Recent advances in bacterial cellulose," *Cellulose*, vol. 21, no. 1. Springer Netherlands, pp. 1–30, 27-Feb-2014.

[28] I. Siró and D. Plackett, "Microfibrillated cellulose and new nanocomposite materials: A review," *Cellulose*, vol. 17, no. 3. Springer Netherlands, pp. 459–494, 21-Jun-2010.

[29] M. A. Hubbe *et al.*, "Nanocellulose in packaging," 2017 .

[30] T. Lindström and C. Aulin, "Market and technical challenges and opportunities in the area of innovative new materials and composites based on nanocellulosics," *Scandinavian Journal of Forest Research*, vol. 29, no. 4. Taylor & Francis, pp. 345–351, 19-May-2014.

[31] A. J. Benítez and A. Walther, "Cellulose nanofibril nanopapers and bioinspired nanocomposites: a review to understand the mechanical property space," *J. Mater. Chem. A*, vol. 5, no. 31, pp. 16003–16024, 2017 .

[32] V. Kumar *et al.*, "Comparison of nano- and microfibrillated cellulose films," *Cellulose*, vol. 21, no. 5, pp. 3443–3456, 2014 .

[33] R. Koppolu, T. Abitbol, V. Kumar, A. K. Jaiswal, A. Swerin, and M. Toivakka, "Continuous roll-to-roll coating of cellulose nanocrystals onto paperboard," *Cellulose*, vol. 25, no. 10, pp. 6055–6069, 2018 .

[34] T. Mäkelä, M. Kainlauri, P. Willberg-Keyriläinen, T. Tammelin, and U. Forsström, "Fabrication of micropillars on nanocellulose films using a roll-to-roll nanoimprinting method," *Microelectron. Eng.*, vol. 163, pp. 1–6, 2016 .

[35] H. M. C. Azeredo, M. F. Rosa, and L. H. C. Mattoso, "Nanocellulose in bio-based food packaging applications," *Industrial Crops and Products*, vol. 97, no. Supplement C. pp. 664–671, 2017.

[36] C. Aulin, M. Gällstedt, and T. Lindström, "Oxygen and oil barrier properties of microfibrillated cellulose films and coatings."

[37] K. L. Spence, R. A. Venditti, O. J. Rojas, J. J. Pawlak, and M. A. Hubbe, "Water vapor barrier properties of coated and filled microfibrillated cellulose composite films," *BioResources*, vol. 6, no. 4, pp. 4370–4388, 2011 .

[38] K. Syverud and P. Stenius, "Strength and barrier properties of MFC films," *Cellulose*, vol. 16, no. 1, pp. 75–85, 2009 .

[39] H. Song, M. Ankerfors, M. Hoc, and T. Lindström, "Reduction of the linting and dusting propensity of newspaper using starch and microfibrillated cellulose," *Nord. Pulp Pap. Res. J.*, vol. 25, pp. 495–504, 2010 .

[40] H. Hamada and D. Bousfield, "Nanofibrillated cellulose as a coating agent to improve print quality of synthetic fiber sheets," *Tappi J.*, vol. 9, pp. 25–29, 2010 .

[41] V. Kumar, "Roll-to-roll processing of nanocellulose into coatings," Åbo

Akademi University, 2018.

[42] R. Koppolu, T. Abitbol, V. Kumar, A. K. Jaiswal, A. Swerin, and M. Toivakka, “Continuous roll-to-roll coating of cellulose nanocrystals onto paperboard,” *Cellulose*, pp. 1–15, 2018 .

[43] L. Cartz, *Nondestructive Testing*. 1995.

[44] E. Terzic, J. Terzic, R. Nagarajah, and M. Alamgir, “A neural network approach to fluid quantity measurement in dynamic environments,” *A Neural Netw. Approach to Fluid Quant. Meas. Dyn. Environ.*, vol. 9781447140, pp. 1–138, 2012 .

[45] T. O. Kim, H. Y. Kim, C. M. Kim, and J. H. Ahn, “Non-Contact and In-Process Measurement of Film Coating Thickness by Combining Two Principles of Eddy-Current and Capacitance Sensing,” *CIRP Ann.*, vol. 56, no. 1, pp. 509–512, 2007 .

[46] J. Seong, S. Kim, J. Park, D. Lee, and K. H. Shin, “Online noncontact thickness measurement of printed conductive silver patterns in Roll-to-Roll gravure printing,” *Int. J. Precis. Eng. Manuf.*, vol. 16, no. 11, pp. 2265–2270, 2015 .

[47] Fischer Technology, “Coating thickness measurement using induction.” [Online]. Available: https://www.fischer-technology.com/en/united-states/knowledge/methods/coating-thickness-measurement/magnetic-induction-process/. [Accessed: 10-Jan-2019].

[48] W. Yin and A. J. Peyton, “Thickness measurement of non-magnetic plates using multi-frequency eddy current sensors,” *NDT E Int.*, vol. 40, no. 1, pp. 43–48, 2007 .

[49] H.-C. Yang and C.-C. Tai, “Pulsed eddy-current measurement of a conducting coating on a magnetic metal plate,” *Meas. Sci. Technol.*, vol. 13, no. 8, p. 1259, 2002 .

[50] W. Li, H. Wang, and Z. Feng, “Non-contact online thickness measurement system for metal films based on eddy current sensing with distance tracking technique,” *Rev. Sci. Instrum.*, vol. 87, no. 4, p. 45005, 2016 .

[51] C. S. Angani, D. G. Park, C. G. Kim, P. Leela, P. Kollu, and Y. M. Cheong, “The pulsed eddy current differential probe to detect a thickness variation in an insulated stainless steel,” *J. Nondestruct. Eval.*, vol. 29, no. 4, pp. 248–252, 2010 .

[52] J. Kral, R. Smid, H. Ramos, and A. Ribeiro, “The Lift-Off Effect in Eddy Currents on Thickness Modeling and Measurement,” *Instrum. Meas. IEEE Trans.*, vol. 62, pp. 2043–2049, 2013 .

[53] F. Tojo *et al.*, “Highly accurate measurement of sheet thickness: The planar error correction,” in *IEEE Transactions on Applied Superconductivity*, 2004, vol. 14, no. 2, pp. 1810–1813.

[54] K. Pacaphol and D. Aht-Ong, “The influences of silanes on interfacial adhesion and surface properties of nanocellulose film coating on glass and aluminum substrates,” *Surf. Coatings Technol.*, vol. 320, pp. 70–81, 2017 .

[55] W. Ledger, *Practical organic coatings analysis*. 2002.

[56] B. H. Stuart, B. George, and P. McIntyre, *Modern Infrared Spectroscopy*. Wiley, 1996.

[57] F. T. Walder, D. W. Vidrine, and G. C. Hansen, "The Analysis of Lubricants on Magnetic Disks by Fourier Transform Infrared Spectroscopy," *Appl. Spectrosc.*, vol. 38, no. 6, pp. 782–786, 1984 .

[58] A. M. C. Davies, A. Grant, G. M. Gavrel, and R. V Steeper, "Rapid analysis of packaging laminates by near-infrared spectroscopy," *Analyst*, vol. 110, no. 6, pp. 643–647, 1985 .

[59] P. Rosenthal A and P. Solomon R, "Spectrometric Method For Analysis Of Film Thickness and Composition on a Patterned Sample," WO1998US25996 19981207, 1999.

[60] A. P. Cherkassky, "Method and apparatus for non-destructive determination of film thickness and dopant concentration using fourier transform infrared spectrometry," US6242739B1, 19-Apr-1999.

[61] V. P. Tolstoy, I. V Chernyshova, and V. A. Skryshevsky, *Handbook of Infrared Spectroscopy*. 2003.

[62] D. Wang, Y. Yang, and J. Zou, "New correction method for FTIR online film-thickness measurement," 1996, vol. 2857, no., pp. 2857–2859.

[63] C. D. Clark and J. H. Crawford, "The interaction of colour centres and dislocations," *Adv. Phys.*, vol. 22, no. 2, pp. 117–205, 1973 .

[64] M. Lubnow, J. B. Jeffries, T. Dreier, and C. Schulz, "Water film thickness imaging based on time-multiplexed near-infrared absorption," *Opt. Express*, vol. 26, no. 16, p. 20902, 2018 .

[65] R. F. Edgar and P. H. Hindle, "New Correlation For On-Line Film Thickness Measurement," *Opt. Eng.*, vol. 27, no. 1, pp. 270150–270155, 1988 .

[66] B. D. Teolis, M. J. Loeffler, U. Raut, M. Famá, and R. A. Baragiola, "Infrared reflectance spectroscopy on thin films: Interference effects," *Icarus*, vol. 190, no. 1, pp. 274–279, 2007 .

[67] M. Bass and V. Freger, "Facile evaluation of coating thickness on membranes using ATR-FTIR," *J. Memb. Sci.*, vol. 492, pp. 348–354, 2015 .

[68] M. D. Mowery, R. Sing, J. Kirsch, A. Razaghi, S. Béchard, and R. A. Reed, "Rapid at-line analysis of coating thickness and uniformity on tablets using laser induced breakdown spectroscopy," *J. Pharm. Biomed. Anal.*, vol. 28, no. 5, pp. 935–943, 2002 .

[69] R. P. Cogdill *et al.*, "Comparison of Terahertz Pulse Imaging and Near-Infrared Spectroscopy for Rapid, Non-Destructive Analysis of Tablet Coating Thickness and Uniformity," *J. Pharm. Innov.*, vol. 2, no. 1, pp. 29–36, 2007 .

[70] Y.-C. Shen, "Terahertz pulsed spectroscopy and imaging for pharmaceutical applications: A review," *Int. J. Pharm.*, vol. 417, no. 1–2, pp. 48–60, 2011 .

[71] Y.-K. Zhu, G.-Y. Tian, R.-S. Lu, and H. Zhang, "A review of optical NDT technologies," *Sensors (Basel).*, vol. 11, no. 8, pp. 7773–7798, 2011 .

[72] InfraTec LLC, "Thermography in the plastics industry." [Online]. Available: https://www.infratec-infrared.com/thermography/industries-applications/plastics-industry/. [Accessed: 23-Jan-2019].

[73] S. A. Martsinukov, D. K. Kostrin, V. V Chernigovskiy, and A. A. Lisenkov, "Measurement of coating thickness using laser heating," *J. Phys. Conf. Ser.*, vol. 735, no. 1, p. 012049, 2016 .

[74] J. Opsal, A. Rosencwaig, and D. L. Willenborg, "Thermal-wave detection and thin-film thickness measurements with laser beam deflection," *Appl. Opt.*, vol. 22, no. 20, p. 3169, 1983 .

[75] S. Mezghani, E. Perrin, V. Vrabie, J. L. Bodnar, J. Marthe, and B. Cauwe, "Evaluation of paint coating thickness variations based on pulsed Infrared thermography laser technique," *Infrared Phys. Technol.*, vol. 76, pp. 393–401, 2016 .

[76] E. Welsch and D. Ristau, "Photothermal measurements on optical thin films," *Appl. Opt.*, vol. 34, no. 31, pp. 7239–7253, 1995 .

[77] F. Maier and B. G. Zagar, "Measurement of paint coating thickness by thermal transient method," in *IEEE Transactions on Instrumentation and Measurement*, 2009, vol. 58, no. 6, pp. 1958–1966.

[78] P. Sadooghi, "Transient coupled radiative and conductive heat transfer in a semitransparent layer of ceramic," *J. Quant. Spectrosc. Radiat. Transf.*, vol. 92, no. 4, pp. 403–416, 2005 .

[79] V. G. Zverev, V. D. Goldin, and A. V Teploukhov, "Physical and Mathematical Modeling of Heat Transfer in Intumescent Thermal Protective Coatings Under Radiative Heating," *IOP Conf. Ser. Mater. Sci. Eng.*, vol. 127, no. 1, p. 012009, 2016 .

[80] H. Halloua *et al.*, "Neural networks and genetic algorithms for the evaluation of coatings thicknesses in thermal barriers by infrared thermography data," *Procedia Struct. Integr.*, vol. 5, pp. 997–1004, 2017 .

[81] R. Shrestha and W. Kim, "Evaluation of coating thickness by thermal wave imaging: A comparative study of pulsed and lock-in infrared thermography – Part I: Simulation," *Infrared Phys. Technol.*, vol. 83, pp. 124–131, 2017 .

[82] R. Shrestha and W. Kim, "Non-destructive testing and evaluation of materials using active thermography and enhancement of signal to noise ratio through data fusion," *Infrared Phys. Technol.*, vol. 94, pp. 78–84, 2018 .

[83] Erichsen GmbH, "Coating Thickness Gauge LayerScan 590-1000." [Online]. Available: https://www.erichsen.de/surfacetesting/film-thickness/coating-thickness-gauge-layerscan-590/coating-thickness-gauge-layerscan-590-1000. [Accessed: 11-Feb-2019].

[84] N. Reinke and A. Bariska, "Device for the Contactless and Non-Destructive Testing of Surfaces," 20130037720, 2013.

[85] A. Bleuler, J. Storskogen, N. Salihi, and N. Reinke, "Device for the Contactless and Non-Destructive Testing of a Surface by Measuring its Infrared Radiation," US20170356844A1, 09-Jun-2017.

[86] B. J. Biddles and D. R. Lobb, "Optical Methods of Thickness Measurement," *IFAC Proc. Vol.*, vol. 4, no. 1, pp. 484–492, 1971 .

[87] J. P. Peterson and R. B. Peterson, "Laser triangulation for liquid film thickness measurements through multiple interfaces," *Appl. Opt.*, vol. 45, no. 20, p. 4916, 2006 .

[88] KEYENCE America, "1D Laser Displacement Sensors Measurement Library." [Online]. Available: https://www.keyence.com/ss/products/measure/measurement_library/type/laser_1d/. [Accessed: 13-Feb-2019].

[89] V. N. Khramov and A. Adamov, "Modification of the laser triangulation method for measuring the thickness of optical layers," in *Saratov Fall Meeting 2017: Laser Physics and Photonics XVIII; and Computational Biophysics and Analysis of Biomedical Data IV*, 2018, vol. 10717, p. 87.

[90] K. B. Smith and Y. F. Zheng, "Accuracy Analysis of Point Laser Triangulation Probes Using Simulation," *J. Manuf. Sci. Eng.*, vol. 120, no. 4, p. 736, 1998 .

[91] F. Murakami, "Accuracy assessment of a laser triangulation sensor," in *Instrumentation and Measurement Technology Conference, 1994. IMTC/94. Conference Proceedings. 10th Anniversary. Advanced Technologies in I & M., 1994 IEEE*, 1994, pp. 802–805.

[92] R. G. Dorsch, G. Häusler, and J. M. Herrmann, "Laser triangulation: fundamental uncertainty in distance measurement," *Appl. Opt.*, vol. 33, no. 7, p. 1306, 1994 .

[93] T. A. Shedd and T. A. Newell, "Automated optical liquid film thickness measurement method," *Rev. Sci. Instrum.*, vol. 69, no. 12, pp. 4205–4213, 1998 .

[94] P. A. Flournoy, R. W. McClure, and G. Wyntjes, "White-Light Interferometric Thickness Gauge," *Appl. Opt.*, vol. 11, no. 9, p. 1907, 1972 .

[95] W. M. Nozhat, "Measurement of liquid-film thickness by laser interferometry," *Appl. Opt.*, vol. 36, no. 30, p. 7864, 1997 .

[96] H. Nouira, N. El-Hayek, X. Yuan, N. Anwer, and J. Salgado, "Metrological characterization of optical confocal sensors measurements (20 and 350 travel ranges)," in *Journal of Physics: Conference Series*, 2014, vol. 483, no. 1, p. 12015.

[97] Micro-Epsilon, "How to Get the Optimum Measurements Using Confocal Sensor," 2018. [Online]. Available: https://www.azosensors.com/article.aspx?ArticleID=1174. [Accessed: 13-Feb-2019].

[98] A. Naderi and T. Lindström, "A comparative study of the rheological properties of three different nanofibrillated cellulose systems," *Nord. Pulp*

Pap. Res. J., vol. 31, no. 3, pp. 354–363, 2016 .

[99] V. Kumar, B. Nazari, D. Bousfield, and M. Toivakka, “Rheology of microfibrillated cellulose suspensions in pressure-driven flow,” *Appl. Rheol.*, vol. 26, no. 4, p. 43534, 2016 .

[100] A. Karppinen, T. Saarinen, J. Salmela, A. Laukkanen, M. Nuopponen, and J. Seppälä, “Flocculation of microfibrillated cellulose in shear flow,” *Cellulose*, vol. 19, no. 6, pp. 1807–1819, 2012 .

7. Appendices

Appendix A

Table A- 1: Error in measurements for wet coatings using NIR spectroscopy

Film Material	Substrate	Knife gap used (µm)	Absolute Error (µm)	Error (%)
CNF	Steel	700	-178	32
	Steel	300	44	22
	Steel	100	N/A	N/A
	Membrane	700	116	18
	Membrane	300	-151	76
	Membrane	100	-325	650
	Plastic	700	-85	15
	Plastic	300	78	28
	Plastic	100	N/A	N/A
MFC	Steel	700	-114	21
	Steel	300	-46	23
	Steel	100	-44	147
	Membrane	700	-64	10
	Membrane	300	-220	110
	Membrane	100	-22	55
	Plastic	700	-71	13
	Plastic	300	79	29
	Plastic	100	-23	92

Table A- 2: Error in measurements for dry coatings using NIR spectroscopy

Film Material	Substrate	Knife gap used (µm)	Absolute Error (µm)	Error (%)
CNF	Steel	700	-19	158
	Steel	300	-33	471
	Steel	100	N/A	N/A
	Membrane	700	-26	236
	Membrane	300	-29	725
	Membrane	100	-32	1600
	Plastic	700	-17	283
	Plastic	300	5	100
	Plastic	100	N/A	N/A
MFC	Steel	700	-17	121
	Steel	300	-28	245
	Steel	100	-48	567
	Membrane	700	-54	245
	Membrane	300	-30	250
	Membrane	100	-37	617
	Plastic	700	-48	253
	Plastic	300	-37	463
	Plastic	100	-34	567

Table A- 3: Error in measurements for wet coatings using IR thermography

Film Material	Substrate	Knife gap used (µm)	Absolute Error (µm)	Error (%)
CNF	Steel	700	147	27
	Steel	500	-6	2
	Steel	300	4	3
	Membrane	700	66	26
	Membrane	500	-157	70
	Membrane	300	5	10
	Plastic	700	28	5
	Plastic	500	-43	9
	Plastic	300	-106	38
MFC	Steel	700	-114	21
	Steel	500	-37	8
	Steel	300	-50	21
	Membrane	700	15	3
	Membrane	500	-233	61
	Membrane	300	-140	78
	Plastic	700	-43	7
	Plastic	500	-230	49
	Plastic	300	-280	108

Table A- 4: Error in measurements for dry coatings using IR thermography

Film Material	Substrate	Knife gap used (µm)	Absolute Error (µm)	Error (%)
CNF	Steel	700	2.7	38
	Steel	500	0.4	9.3
	Steel	300	0.3	10.7
	Membrane	700	-10.3	90.4
	Membrane	500	-13.4	372.2
	Membrane	300	-2.5	125
	Plastic	700	-2.4	38.7
	Plastic	500	-3.0	65.2
	Plastic	300	-2.8	77.8
MFC	Steel	700	-2.6	18.3
	Steel	500	5.8	50.2
	Steel	300	1.8	21.8
	Membrane	700	-8.7	47.2
	Membrane	500	-1.1	7.5
	Membrane	300	-14	152.3
	Plastic	700	7.1	40.1
	Plastic	500	12.2	79.3
	Plastic	300	5.7	74.5

Table A- 5: Error in measurements for wet coatings using optical confocal method

Film Material	Substrate	Knife gap used (µm)	Absolute Error (µm)	Error (%)
CNF	Steel	700	523	95
	Steel	500	370	97
	Steel	300	118	98
	Membrane	700	246	98
	Membrane	500	221	98
	Membrane	300	48	96
	Plastic	700	482	80
	Plastic	500	383	82
	Plastic	300	242	86
MFC	Steel	700	-66	-12
	Steel	500	-4	-1
	Steel	300	-17	-7
	Membrane	700	-6	-1
	Membrane	500	28	7
	Membrane	300	-79	-44
	Plastic	700	19	3
	Plastic	500	-1	0
	Plastic	300	36	14

Table A- 6: Error in measurements for dry coatings using optical confocal method

Film Material	Substrate	Knife gap used (µm)	Absolute Error (µm)	Error (%)
CNF	Steel	700	3.2	45.1
	Steel	500	0.6	14.2
	Steel	300	1.5	52.9
	Membrane	700	2.1	18.6
	Membrane	500	-3.4	93.8
	Membrane	300	-0.7	35.9
	Plastic	700	5.4	87.1
	Plastic	500	4.0	87
	Plastic	300	3.5	97.2
MFC	Steel	700	-5.2	37.2
	Steel	500	-0.6	5
	Steel	300	5.3	63.2
	Membrane	700	-0.7	3.9
	Membrane	500	4.7	31.4
	Membrane	300	3.9	42.4
	Plastic	700	-4.7	26.7
	Plastic	500	3.2	20.6
	Plastic	300	-3.2	41.8